

Modeling Diversity Dynamics in Time-Evolving Collaboration Networks

*Christopher Archer
Gireeja Ranade, Ed.*



Electrical Engineering and Computer Sciences
University of California, Berkeley

Technical Report No. UCB/EECS-2025-122

<http://www2.eecs.berkeley.edu/Pubs/TechRpts/2025/EECS-2025-122.html>

May 17, 2025

Copyright © 2025, by the author(s).
All rights reserved.

Permission to make digital or hard copies of all or part of this work for personal or classroom use is granted without fee provided that copies are not made or distributed for profit or commercial advantage and that copies bear this notice and the full citation on the first page. To copy otherwise, to republish, to post on servers or to redistribute to lists, requires prior specific permission.

Acknowledgement

Thanks to Gireeja Ranade for her advisorship. Thanks to Benjamin Recht, Ebonye Smith, Sultan Daniels, Eric Xu, Manooshree Patel, and Moses Won for their review and critique. Thanks to the Berkeley Algorithms, Data, and Society Reading Group for their guidance. I also would like to thank my family, Shivaun, Lynden, and Cairo Archer.

Modeling Diversity Dynamics in Time-Evolving Collaboration Networks

by

Christopher Archer

A thesis submitted in partial satisfaction of the
requirements for the degree of

Masters of Science

in

Electrical Engineering & Computer Sciences

in the

Graduate Division

of the


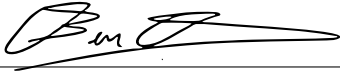
University of California, Berkeley

Committee in charge:

Professor Gireeja Ranade, Chair
Professor Benjamin Recht

Spring 2025

The thesis of Christopher Archer, titled Modeling Diversity Dynamics in Time-Evolving Collaboration Networks, is approved:

Chair		Date	May 16, 2024
		Date	May 16, 2024
		Date	

University of California, Berkeley

Modeling Diversity Dynamics in Time-Evolving Collaboration Networks

Copyright 2025
by
Christopher Archer

MODELING DIVERSITY DYNAMICS IN TIME-EVOLVING COLLABORATION NETWORKS

MASTER’S THESIS

 **Christopher Archer***

Department of Electrical Engineering & Computer Sciences
University of California, Berkeley
Berkeley, CA 94702
chris_archer@berkeley.edu

May 16, 2025

ABSTRACT

Increasing diversity in a community or an organization requires paying attention to many different aspects, including recruitment, hiring, retention, climate, and more. In this paper, we focus on how climate, captured through network interactions, can affect the growth or decay of minority populations within that community. Building on previous work, we develop a dynamic stochastic block model that grows according to a weighted version of preferential attachment, while having some memory of previous edges as well. This models how interactions between nodes in the network can influence the recruitment of new nodes to the network. We derive a deterministic approximation of this random system and prove its convergence is determined by the network parameters. Additionally, we show how the memory of the network affects convergence under different parameter regimes, and we validate this model by assessing the growth of women scientists in the American Physics Society’s co-authorship network. We conclude with two extensions to the model, accounting for "soft" homophily in recruitment as well as node departures.

1 Introduction

While efforts have been made since the 1920s to desegregate and diversify the workplace, modern notions of diversity primarily originate from policies in the 1960s during the Civil Rights Era [20]. The Civil Rights Act of 1964 put an end to the “de facto” policies that discriminated against classes of workers [15]. The benefits of diverse organizations are well-documented; studies and computational experiments show that diverse organizations have increased feelings of belonging and satisfaction amongst workers, and increased problem-solving ability [16, 22].

There has been a large body of work in recent years that has focused on how hiring practices can be amended to be more inclusive and support diversity [32, 39, 44, 28, 36, 47]. However, real-world experience shows that many times so-called “inclusive hiring” programs can mask deeply entrenched social biases that still privilege the status quo [26, 10].

In addition to hiring, growing diversity in an organization also requires focusing on what happens after someone is hired. Harvard Business Review reports that U.S. companies invest a total of 8 billion dollars on Diversity, Equity, and Inclusion (DEI) trainings per year [25]. However, studies show that there remains a large problem with diversity in these organizations [5, 37, 26].

Culture is a huge part of an individual’s experience in a community. An institution that does a good job of recruiting under-represented people but does not have a climate that encourages their retention will ultimately revert to the status quo [6]. In this paper, we explore the connection between the growth of diversity in a community and the connections and collaborations among the people in the community.

*Thanks to Gireeja Ranade for her advisorship. Thanks to Benjamin Recht, Ebonye Smith, Sultan Daniels, Eric Xu, Manooshree Patel, and Moses Won for their review and critique. Thanks to the Berkeley Algorithms, Data, and Society Reading Group for their guidance. I also would like to thank my family, Shivaun, Lynden, and Cairo Archer.

Network analysis allows a way to link “micro-scale” interactions to “macro-scale” organizational structure and dynamics [18, 34, 27]. In this sense, the key micro-scale insight about organizational networks is that in recruiting, people tend to favor candidates similar to them, or those who fit the dominant culture of the organization [42, 10]. The employee referral system, hiring bias, and the infamous “culture fit” qualification are all examples of this phenomenon [42, 43]. As an organization’s network grows in this way, it tends to reproduce the demographics already present in the network. This is known as *homophily*, a term developed to capture how interpersonal networks tend to self-cluster around shared characteristics [34]. In the context of networks, this can be captured through the notion of preferential attachment [8], a weighted version of which we use in this paper.

It has been shown that social ties and networks can impact employment [13, 48] and education outcomes [14]. This property is important to consider for diversity because networks with strong homophily tend to become less diverse over time [2, 43]. We wish to create a model that can capture this phenomenon, and demonstrate how under certain network conditions, it can be prevented. Analysis like this creates an opening for researchers to go beyond assessing inclusive policies from a purely qualitative standpoint and towards a mathematical characterization of organizational “climate”. Additionally, to validate this model in real-world settings we look towards the coauthorship network of the American Physical Society (APS) from 1980 to 2009, to assess how the collaboration structure has impacted the proportion of women authors in APS.

2 Background and Related Work

Many works try to mathematically assess the dynamics of organizations and their impact on diversity. Some works propose ecological models, particularly ecological theories of affiliation to understand how organizational networks grow over time [33]. Others use agent-based modeling approaches, where agents of different communities will have different access to information and algorithms to solve problems [22, 17]. We will focus on network-oriented approaches.

The classic preferential attachment algorithm for network growth was introduced in [8]. The growth of scientific collaboration networks has been specifically studied in [9, 23]. Strategic perspectives on these collaborations have also been studied in [24]. How network growth relates to the communities formed is studied in [7]. [40] provides a formulation of “social capital” in networks, which defines how value can be generated based on one’s position in a social network, through useful information, personal relationships, or the ability to organize groups. In heterogeneous networks, it has been shown that “broker” nodes with ties that connect clusters and span the “structural holes” of the network have greater access to social capital due to their unique access to diverse information [12]. To this end, measures of “betweenness” in networks have been used as a way to identify which nodes tend to span structural holes [32]. Research has also been done on the strength of weak ties, or connections that are accessed less frequently, in networks. Due to the nature of strong ties being connections that are accessed frequently, much of the information shared in networks of strong ties becomes redundant, and through weak ties, more novel information can be accessed [18].

Recently, [11] utilized the Stochastic Block Model to show how diversity in a heterogeneous network evolves under homophily and preferential attachment. The model in [11] is very similar to the model in [46], which also tries to capture biased network growth through homophily. This model was able to mathematically prove threshold effects under which minority populations would proportionally vanish or reach parity in the network, showing that low cross-community collaboration rates will always lead to the minority vanishing [11]. However, one of the main oversights of this model was its lack of long-term memory. In particular, it was assumed that the network was renewed at every time step. In time-evolving networks, memory is crucial in the understanding of complex temporal systems and can have great influence on emergent properties of the network [41, 35]. Works such as [19] have also explored how memory of social connections influences network communities. Without any encoding of memory, the model dynamics in [11] were essentially a sequence of independent static graphs with new nodes added. This paper’s model seeks to build on [11] with the addition of a “memory” parameter which influences how long edges persist over time steps.

3 Main Contributions

In our paper, we contribute the following:

- (1) Develop a model that builds on [11] that captures how homophily can affect diversity in collaboration networks while accounting for memory in the collaborations (edges) of the graph. We show that certain network conditions can lead to a decline in minority populations (Section 4).

- (2) Characterize the effect memory has on the rate of growth of the minority population and provide parameter regimes where memory can change the fixed point of the system, using a deterministic approximation to the stochastic system (Sections 5 and 6).
- (3) Validate this model on gender diversity in scientific collaborations using the American Physics Society's citation network dataset [1]. In particular, we see in Figure 1 that the best-fit model we propose can roughly predict the growth of the minority population (women) in this dataset. We discuss this figure in more detail in Section 7.
- (4) Mathematically and empirically investigate extensions to the model – the introduction of recruitment via "soft homophily", and investigation of the system with node departures.

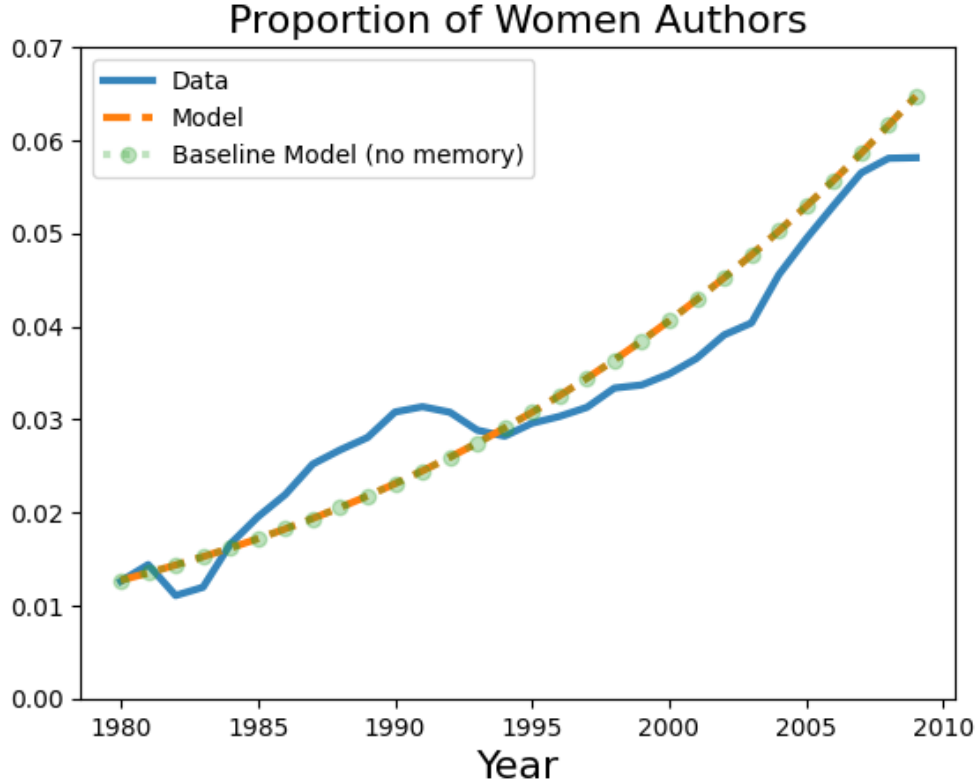


Figure 1: Plot of the proportion of women in the APS co-authorship network from 1980-2009. The best-fit model identified, with memory parameter $q = 0.265$ is shown in orange, and the model from [1], with memory parameter $q = 0$ (i.e. no memory) is shown in green.

4 Model Overview

Our basic model here replicates many of the features of [1]. We consider a Stochastic Block Model with two communities as the underlying structure. Nodes have weights that correspond to their “success” (which is the weighted sum of the collaborations (edges) of the node). Successful nodes are more influential in the recruitment of new nodes to the network (preferential attachment). Homophily plays a key role in recruitment since nodes only recruit members of their own community. The combination of homophily and preferential attachment leads to a rich-get-richer phenomenon, and we are interested in how the minority community evolves over time. We summarize key model features here:

- (i) *Community Structure*: We use a two-community (Red/Blue) Stochastic Block Model to account for differential interactions between different communities.
- (ii) *Collaborations*: In this network model, nodes represent people, and edges between nodes represent collaborations between two people. These edges will be weighted to account for how “successful” a collaboration is.
- (iii) *Node Influence*: The weight of a node is the sum of the weights of all its edges. Nodes with higher weight can recruit more new nodes.

- (iv) *Homophily*: A node will always recruit new nodes of the same color (sub-community). This leads to a rich-get-richer phenomenon since nodes with higher weight tend to recruit more nodes (weighted preferential attachment). The total number of nodes from a community (say red nodes) arriving at a particular time depends on the total weight of red nodes in the graph at the preceding time.
- (v) *Memory*: Given a collaboration network, people who have collaborated in one timestep are more likely to collaborate again in the next timestep. This is the key point of divergence from the model in [11]. While [11] assumed that brand-new collaborations were created at every time step, here we allow collaborations to persist over multiple time steps.

4.1 Weighted Stochastic Block Model

The Stochastic Block Model (SBM) [21] is a generalization of the Erdős-Rényi $G(n, p)$ random graph, which supports the interactions of multiple communities within the graph [30]. Weighted SBMs have been studied in [3, 4, 38]. In this paper, we consider two communities, Red and Blue. Without loss of generality, assume Red is the minority community. To maintain consistency with [11], we mirror much of the notation below.

Definition 4.1 (Weighted Stochastic Block Model). *Let $[n] = \{1, \dots, n\}$ be a set of nodes, where each node $i \in [n]$ has color $c[i] \in \{R, B\}$. Define interaction matrix $\mathbf{P} = \begin{bmatrix} \mu_{RR} & \mu_{RB} \\ \mu_{BR} & \mu_{BB} \end{bmatrix}$ and weight matrix $\mathbf{W} = \begin{bmatrix} w_{RR} & w_{RB} \\ w_{BR} & w_{BB} \end{bmatrix}$ where $\mathbf{P}, \mathbf{W} > 0$. Generate a weighted random graph on $[n]$, so that for every pair of nodes $i, j \in [n]^2$, the edge's weight $w_{i,j} = w_{c[i],c[j]}$ with probability $\mu_{c[i],c[j]}/n$, and otherwise $w_{i,j} = 0$.*

For this paper, we assume our matrices \mathbf{P}, \mathbf{W} are such that $\mu_{RR} = \mu_{BB}, w_{RR} = w_{BB}$ and $\mu_{RB} = \mu_{BR}, w_{RB} = w_{BR}$. Also note that the entries $\mu_{c[i],c[j]}$ of matrix \mathbf{P} are not themselves probabilities. The probability of an edge existing between two nodes is $\mu_{c[i],c[j]}/n$. One can think of $\mu_{c[i],c[j]}$ as the expected number of edges a node of color $c[i]$ will form with nodes of color $c[j]$ in the network without any memory.

4.2 Stochastic Block Model Dynamics

We assume that the recruitment of new nodes to the network happens in discrete time steps, and a constant fraction of new nodes join the network at each time step.

Definition 4.2 (Stochastic Block Model Dynamics). *Let $G_t = (V_t, E_t)$ be our graph at time t . Assume this graph contains n_t nodes, with n_t^R Red nodes and n_t^B Blue nodes. At each time step, $\lceil \lambda n_t \rceil, \lambda > 0$ new nodes are added to the network. Additionally, define edge holdover probability $q \in [0, 1]$. Our procedure for generating the subsequent graph G_{t+1} is as follows:*

- (1) Calculate the total weight of Red nodes and Blue nodes in G_t , defined as $R_t = \sum_{c[i]=R} \sum_{j \in [n_t]} w_{ij}$, and $B_t = \sum_{c[i]=B} \sum_{j \in [n_t]} w_{ij}$.
- (2) Define intermediate graph $G_t^+ = (V_t, E_t^+)$ where for every edge $(i, j) \in E_t$, with probability q let $(i, j) \in E_t^+$, otherwise remove it.
- (3) Add $m_{t+1} := \lceil \lambda n_t \rceil$ new nodes to graph G_t^+ . Each incoming node is Red with probability $\frac{R_t}{R_t + B_t}$, or Blue with probability $\frac{B_t}{R_t + B_t}$.
- (4) Initialize $G_{t+1} = G_t^+$, and for all potential edges $(i, j) \notin E_t^+$, generate them according the Weighted Stochastic Block Model with parameters \mathbf{P} and \mathbf{W} .

The recruitment dynamics in step (3) of Definition 4.2 come from our assumption of homophily and preferential attachment. New Red nodes are recruited by existing Red nodes and arrive proportional to the total weight of Red nodes in the network. The same is true for Blue nodes. Let $w_i = \sum_{j \in [n_t]} w_{ij}$ be the weight of a node i , and $w = \sum_{i \in [n_t]} w_i$ be the total weight of all nodes. Then our recruitment dynamics in step (3) are equivalent to every node i recruiting on average $m_{t+1} \cdot \frac{w_i}{w}$ nodes of the same color.

5 Deterministic Approximation

To understand the stochastic system, we will construct a deterministic approximation that follows the mean of the system. We will show that the stochastic system does not deviate too far from the deterministic system. For this, we first

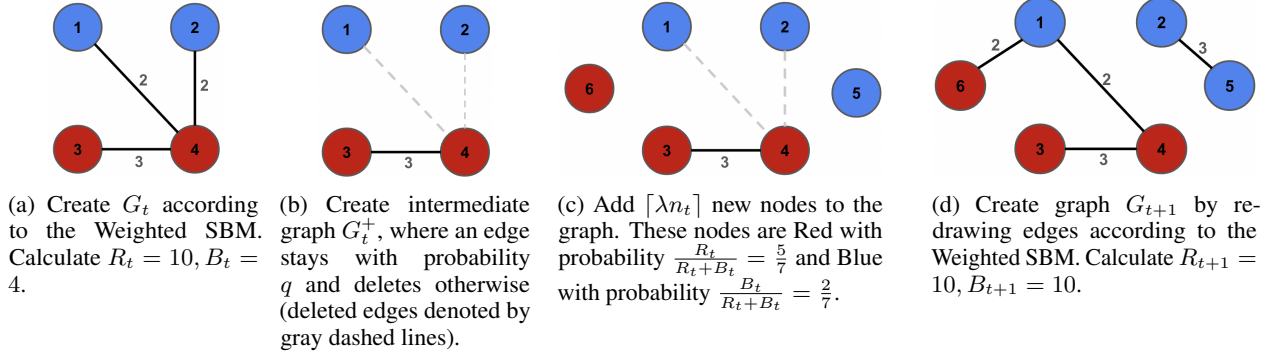


Figure 2: Visualization of the Stochastic Block Model Dynamics described in Definition 4.2 for $\mathbf{P} = \begin{bmatrix} 0.7 & 1 \\ 1 & 0.7 \end{bmatrix}$, $\mathbf{W} = \begin{bmatrix} 3 & 2 \\ 2 & 3 \end{bmatrix}$, $q = 0.5, \lambda = 0.5$. Figure 2a shows initialization of G_t . Figure 2b shows the intermediate graph G_t^+ with some edges persisting according to the q parameter. Figure 2c shows new nodes being added to the network according to preferential attachment, and Figure 2d shows the creation of G_{t+1} according to the Weighted SBM from Definition 4.1.

compute the probability that an edge exists at a given time. Because the graph has memory, the probability of an edge existing at time t is dependent on all previous graphs $\{G_k | k \leq t\}$. We define the event $\mathcal{E}_{ij}(t)$ on each edge $(i, j) \in E_t$, where $\mathcal{E}_{ij}(t) := \{\text{edge } (i, j) \text{ exists at time } t\}$.

Lemma 5.1. Let $\Pi_{RR}(t) := \Pr(\mathcal{E}_{ij}(t) | c[i] = c[j] = R)$. Then:

$$\Pi_{RR}(t) = \frac{\mu_{RR}}{n_t} + \sum_{k=0}^{t-1} \frac{\mu_{RR}}{n_k} \prod_{j=k+1}^t q \left(1 - \frac{\mu_{RR}}{n_j}\right). \quad (1)$$

Proof. Fix edge $(i, j) \in E_t$. Without loss of generality, assume $c[i] = c[j] = R$. We derive the probability of event $\mathcal{E}_{ij}(t)$ by conditioning on the previous timestep $\mathcal{E}_{ij}(t-1)$ with our edge holdover probability q .

$$\Pr(\mathcal{E}_{ij}(t)) = \Pr(\mathcal{E}_{ij}(t) | \mathcal{E}_{ij}(t-1)) \Pr(\mathcal{E}_{ij}(t-1)) + \Pr(\mathcal{E}_{ij}(t) | \mathcal{E}_{ij}^c(t-1)) \Pr(\mathcal{E}_{ij}^c(t-1)) \quad (2)$$

$$= \left(q + (1-q) \frac{\mu_{RR}}{n_t}\right) \Pr(\mathcal{E}_{ij}(t-1)) + \left(\frac{\mu_{RR}}{n_t}\right) (1 - \Pr(\mathcal{E}_{ij}(t-1))) \quad (3)$$

$$= \frac{\mu_{RR}}{n_t} + q \left(1 - \frac{\mu_{RR}}{n_t}\right) \Pr(\mathcal{E}_{ij}(t-1)). \quad (4)$$

This produces a recursive relationship with initial condition $\Pr(\mathcal{E}_{ij}(0)) = \frac{\mu_{RR}}{n_0}$. We solve this inductively, yielding

$$\Pi_{RR}(t) := \Pr(\mathcal{E}_{ij}(t) | c[i] = c[j] = R) = \frac{\mu_{RR}}{n_t} + \sum_{k=0}^{t-1} \frac{\mu_{RR}}{n_k} \prod_{j=k+1}^t q \left(1 - \frac{\mu_{RR}}{n_j}\right). \quad (5)$$

completing the proof. \square

We can similarly define and compute probabilities $\Pi_{RB}(t)$ and $\Pi_{BB}(t)$. Define the minority fraction in the network as

$$(\phi_t)_{t \geq 0} := \frac{n_t^R}{n_t} = \frac{n_t^R}{n_t^R + n_t^B}. \quad (6)$$

Where n_t^R, n_t^B are the number of Red and Blue nodes in the network at time t , respectively.

Lemma 5.2. Assume $\exists \varepsilon \in (0, \frac{1}{2})$ such that $\left(\frac{1}{n_t}\right)^{\frac{1}{2}-\varepsilon} \leq \phi_t \leq \frac{1}{2}$. Let \mathcal{F}_t be a filtration until time t . Let

$$\Gamma_q(x_t) := \frac{x_t^2 w_{RR} \Pi_{RR}(t) + x_t(1-x_t) w_{RB} \Pi_{RB}(t)}{(x_t^2 + (1-x_t)^2) w_{RR} \Pi_{RR}(t) + 2x_t(1-x_t) w_{RB} \Pi_{RB}(t)}. \quad (7)$$

Then, we can bound the conditional expectation of our process $\mathbb{E}[\phi_{t+1}|\mathcal{F}_t]$ as follows:

$$\frac{\phi_t + \frac{\lfloor \lambda n_t \rfloor}{n_t} \cdot \left(1 - \frac{1}{n_t^{\varepsilon/5}}\right) \Gamma_q(\phi_t)}{1 + \frac{\lfloor \lambda n_t \rfloor}{n_t}} \leq \mathbb{E}[\phi_{t+1}|\mathcal{F}_t] \leq \frac{\phi_t + \frac{\lceil \lambda n_t \rceil}{n_t} \cdot \left(1 + \frac{1}{n_t^{\varepsilon/5}}\right) \Gamma_q(\phi_t)}{1 + \frac{\lceil \lambda n_t \rceil}{n_t}}, \quad (8)$$

with probability at least $1 - \frac{8}{\exp(C_1 n_t^\varepsilon)}$, where $C_1 = \min \left\{ \frac{\mu_{RR}}{24}, \frac{\mu_{RB}}{12} \right\}$ and $\varepsilon \in (0, \frac{1}{2})$.

The proof of Lemma 5.2 is given in the Appendix A.1. We notice that the limit as $t \rightarrow \infty$ of the lower and upper bounds in Lemma 5.2 goes to $\frac{\phi_t + \lambda \cdot \Gamma_q(\phi_t)}{1 + \lambda}$. This motivates the consideration of the following deterministic system, Φ_t , to approximate the stochastic system behavior.

Definition 5.3 (Deterministic System). We define the deterministic system Φ_t as:

$$\Phi_{t+1} = \frac{\Phi_t + \lambda \cdot \Gamma_q(\Phi_t)}{1 + \lambda}, \Phi_0 = \frac{n_0^R}{n_0}, \quad (9)$$

where $\Gamma_q(x_t)$ is as before:

$$\Gamma_q(x_t) = \frac{x_t^2 w_{RR} \Pi_{RR}(t) + x_t(1-x_t) w_{RB} \Pi_{RB}(t)}{(x_t^2 + (1-x_t)^2) w_{RR} \Pi_{RR}(t) + 2x_t(1-x_t) w_{RB} \Pi_{RB}(t)}. \quad (10)$$

We derive this expression in more detail in Appendix Sec. A.2

6 Analysis & Discussion of Deterministic System

In this section, we prove the existence of parameter regimes that will dictate the convergence of the deterministic system. Define $\rho_t := \frac{\Pi_{RR}(t) w_{RR}}{\Pi_{RB}(t) w_{RB}}$. This will be a key parameter in our analysis of the system's behavior.

Lemma 6.1. Assume $q(1+\lambda) > 1$, then $\rho := \lim_{t \rightarrow \infty} \frac{w_{RR} \Pi_{RR}(t)}{w_{RB} \Pi_{RB}(t)}$ exists and is defined as $\rho = \frac{w_{RR} \mu_{RR} S_{RR}}{w_{RB} \mu_{RB} S_{RB}}$, where

$$S_{RR} = \sum_{k=0}^{\infty} (q(1+\lambda))^{-k} \prod_{j=k+1}^{\infty} \left(1 - \frac{\mu_{RR}}{n_0} (1+\lambda)^{-j}\right), \quad (11)$$

and we define S_{RB} similarly.

The proof is in Appendix Section A.3. Now, consider the function $f_t : [0, 1] \rightarrow [0, 1]$, such that

$$f_t(x) = \frac{x + \lambda \Gamma_q(x)}{1 + \lambda} = \frac{x + \lambda \left(\frac{x^2 w_{RR} \Pi_{RR}(t) + x(1-x) w_{RB} \Pi_{RB}(t)}{(x^2 + (1-x)^2) w_{RR} \Pi_{RR}(t) + 2x(1-x) w_{RB} \Pi_{RB}(t)} \right)}{1 + \lambda} \quad (12)$$

$$= \frac{2x^3(\rho_t - 1) - x^2(\rho_t - 1)(2 - \lambda) + x(\rho_t + \lambda)}{(1 + \lambda)(2x^2(\rho_t - 1) - 2x(\rho_t - 1) + \rho_t)}. \quad (13)$$

The simplifications above follow from algebra. $f_t(x)$ captures the update function for the deterministic system in Def. 5.3. We establish the following properties of f_t .

Lemma 6.2. $f_t(x)$ converges uniformly to $f(x)$ as $t \rightarrow \infty$, where

$$f(x) = \frac{2x^3(\rho - 1) - x^2(\rho - 1)(2 - \lambda) + x(\rho + \lambda)}{(1 + \lambda)(2x^2(\rho - 1) - 2x(\rho - 1) + \rho)}.$$

Proof. The denominator of $f_t(x)$ is $(1 + \lambda)(2x^2(\rho_t - 1) - 2x(\rho_t - 1) + \rho_t)$. This denominator is quadratic, with discriminant

$$D = 4(1 + \lambda)^2(\rho_t - 1)^2 - 4(2)(1 + \lambda)^2(\rho_t - 1)\rho_t = -4(1 + \lambda)^2(\rho_t^2 - 1). \quad (14)$$

In the case of $\rho_t > 1$, we have $D < 0$, meaning $f_t(x)$ is strictly bounded away from 0 for all $x \in \mathbb{R}$. For $\rho_t = 1$, our denominator is simply $(1 + \lambda)\rho_t$, and we have $\rho_t > 0$ by assumption. However, in the case of $\rho_t \in (0, 1)$, we see that the discriminant $D > 0$ and the denominator of $f_t(x)$ has real roots. We show that these roots must lie outside the domain of $f_t(x)$, and thus do not impact its convergence.

To prove this, assume $\rho_t \in (0, 1)$. By the quadratic formula the denominator of $f_t(x)$ has roots x_1, x_2 , defined as

$$x_1, x_2 = \frac{2(\rho_t - 1) \pm \sqrt{-4(\rho_t^2 - 1)}}{4(\rho_t - 1)}. \quad (15)$$

We first show that $x_1 := \frac{2(\rho_t - 1) + \sqrt{-4(\rho_t^2 - 1)}}{4(\rho_t - 1)} < 0$. This is equivalent to proving $2(\rho_t - 1) + \sqrt{-4(\rho_t^2 - 1)} > 0$. We construct the following chain of implications

$$2(\rho_t - 1) + \sqrt{-4(\rho_t^2 - 1)} > 0 \quad (16)$$

$$\iff -2(\rho_t - 1) < \sqrt{-4(\rho_t^2 - 1)} \quad (17)$$

$$\iff 2(1 - \rho_t) < 2\sqrt{1 - \rho_t^2}. \quad (18)$$

Since $\rho_t \in (0, 1)$, we know both $1 - \rho_t < 1 - \rho_t^2$, and $1 - \rho_t^2 < \sqrt{1 - \rho_t^2}$, thus proving the claim. To show that $x_2 := \frac{2(\rho_t - 1) - \sqrt{-4(\rho_t^2 - 1)}}{4(\rho_t - 1)} > 1$, we aim to prove the equivalent statement $2(\rho_t - 1) - \sqrt{-4(\rho_t^2 - 1)} < 4(\rho_t - 1)$. Again we construct a chain of implications.

$$2(\rho_t - 1) - \sqrt{-4(\rho_t^2 - 1)} < 4(\rho_t - 1) \quad (19)$$

$$\iff \sqrt{-4(\rho_t^2 - 1)} > -2(\rho_t - 1). \quad (20)$$

Inequality (20) is identical to (17), thus proving the claim. Since we have shown that no roots can exist in the denominator of $f_t(x)$ for $x \in [0, 1]$, we can express the limit as follows:

$$\lim_{t \rightarrow \infty} f_t(x) = \frac{\lim_{t \rightarrow \infty} 2x^3(\rho_t - 1) - x^2(\rho_t - 1)(2 - \lambda) + x(\rho_t + \lambda)}{\lim_{t \rightarrow \infty} (1 + \lambda)(2x^2(\rho_t - 1) - 2x(\rho_t - 1) + \rho_t)} \quad (21)$$

$$= \frac{2x^3(\rho - 1) - x^2(\rho - 1)(2 - \lambda) + x(\rho + \lambda)}{(1 + \lambda)(2x^2(\rho - 1) - 2x(\rho - 1) + \rho)}. \quad (22)$$

which gives the desired result. \square

Lemma 6.3. For any fixed t , if $0 < x < 1/2$:

(1) If $\rho_t > 1$, then $f_t(x) < x$.

(2) If $\rho_t < 1$, then $f_t(x) > x$.

(3) If $\rho_t = 1$, $f_t(x) = x$.

Similarly, if $0 < x < 1/2$

(1) If $\rho > 1$, then $f(x) < x$.

(2) If $\rho < 1$, then $f(x) > x$.

(3) If $\rho = 1$, $f(x) = x$.

The proof of this follows similarly to (11) and is omitted.

Lemma 6.4. $f(x)$ has fixed points at $x = \{0, \frac{1}{2}, 1\}$ if $\rho \neq 1$. If $\rho = 1$, then $f(x) = x \forall x$. Furthermore, for $x \in (0, 1/2)$ the function $f(x)$ monotonically converges to 0 when $\rho > 1$, monotonically converges to $1/2$ when $\rho < 1$, and remains constant if $\rho = 1$.

The proof follows directly from (11) and is omitted.

Theorem 6.5.

- If $\rho > 1$, the deterministic system Φ_t will converge to 0.
- If $\rho < 1$, the deterministic system Φ_t will converge to $\frac{1}{2}$.

Proof. If $\rho > 1$, then there exists T_0 where we have $\rho_t > 1$ for $t \geq T_0$. Thus for $t > T_0$ Lemma 6.3 implies that $\Phi_{t+1} < \Phi_t$. Since $\Phi_t \in [0, 1/2]$ is monotonically strictly decreasing, it must converge to a limit. We claim that this limit must be 0.

For contradiction, let Φ_t converge to $\alpha > 0$. Since Φ_t is decreasing it must converge from the right and there exists T_1 such that for $t > T_1$, we have $\Phi_t > \alpha$.

Let $f(\alpha) = \beta < \alpha$, by Lemma 6.3. By the continuity of f , we have a neighborhood of α such that for all x in that neighborhood, $f(x)$ is arbitrarily close to β . Hence, there exists δ such that

$$f(\alpha + \delta_1) < \alpha - \frac{\alpha - \beta}{2} \quad (23)$$

for all $\delta_1 \in (0, \delta)$.

Lemma 6.2 implies that f_t converges uniformly to f , and there exists T_2 such that for $t > T_2$, we have $|f_t(x) - f(x)| < \frac{\alpha - \beta}{4}$ for all x . Note that $f_t(\Phi_t) = \Phi_{t+1}$ by definition of the update function $f_t(x)$, so we have

$$|f_t(\Phi_t) - f(\Phi_t)| = |\Phi_{t+1} - f(\Phi_t)| < \frac{\alpha - \beta}{4}. \quad (24)$$

Consider $\Phi_t \in (\alpha, \alpha + \delta)$ for $t > \max\{T_0, T_1, T_2\}$. We combine equations (23) and (24) to get:

$$\Phi_{t+1} < f(\Phi_t) + \frac{\alpha - \beta}{4} < \alpha - \frac{\alpha - \beta}{2} + \frac{\alpha - \beta}{4} < \alpha. \quad (25)$$

But this is a contradiction, and therefore Φ_t must converge to 0. A similar argument holds in the case of $\rho < 1$. \square

6.1 The Role of Memory in the Deterministic Approximation

This paper considers a memory parameter q , which is the probability that an edge from one time step persists to the next time step, and this is the primary extension to the model in [11]. Define $\rho_0 := \frac{\mu_{RR} w_{RR}}{\mu_{RB} w_{RB}}$, which is the threshold parameter of the model in [11] with $q = 0$, as well as the value of ρ_t at $t = 0$.

In the case that $\rho_0 \neq 1$, we empirically observe that the value of q only changes the convergence rate of the system to a particular fixed point, and does not change the fixed point itself (Figure 3). In Figure 3a we see that since $\mu_{RR} < \mu_{RB}$ and $\rho_0 < 1$, increasing q causes our process to converge to $\frac{1}{2}$ at a slower rate. In Figure 3b we see that $\mu_{RR} > \mu_{RB}$ and $\rho_0 > 1$, therefore increasing q causes the process to converge to 0 slower. Additionally, we see that for $q \in \{0, 0.5, 0.75\}$, the approximation trajectories are all roughly the same. It is only once $q \in \{0.95, 1.0\}$ that the approximation starts to noticeably differ in its trajectory.

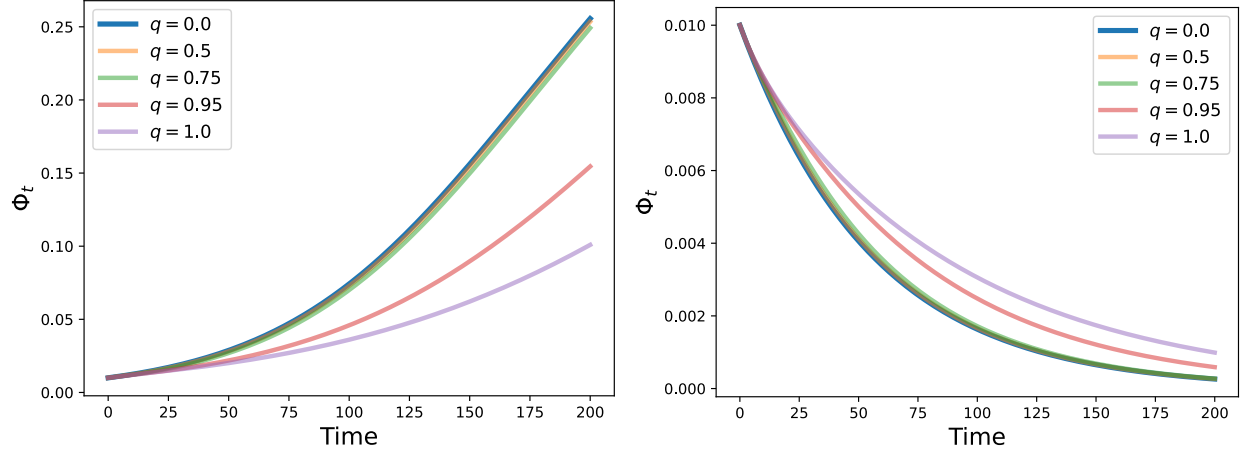
In the case where $\rho_0 = 1$, in the absence of any memory the fraction of the minority will remain constant. However, we see that the inclusion of memory propels the system towards a fixed point (i.e. reaching parity or vanishing). In Figure 4 we see with $\mu_{RR} > \mu_{RB}$ and $\rho_0 = 1$, that increasing q causes the once stationary process to converge to $\frac{1}{2}$. Figure 4b plots the limit point of the deterministic process Φ_∞ over different values of our memory parameter q . Φ_{1000} is used as an approximation for Φ_∞ . We see that a phase transition happens soon after q crosses 0.9. We summarize these observations in Table 1.

Table 1: The convergence of the system with memory in comparison with the memoryless baselines model from [11].

	Baseline model [11]	$\mu_{RR} < \mu_{RB}$	$\mu_{RR} > \mu_{RB}$	$\mu_{RR} = \mu_{RB}$
$\rho_0 > 1$	Converges to 0	Faster to 0	Slower to 0	No change
$\rho_0 < 1$	Converges to $\frac{1}{2}$	Slower to $\frac{1}{2}$	Faster to $\frac{1}{2}$	No change
$\rho_0 = 1$	Constant	Converges to 0	Converges to $\frac{1}{2}$	No change

From Figure 4 we see when $\rho_0 = 1$, meaning the memoryless model would remain static, increasing q changes the system towards convergence to $\frac{1}{2}$. In other words, the proportion of the minority community changed from being stagnant to reaching parity as memory increased. Moreover, we observe that this change in convergence happens suddenly once the memory parameter q crosses a threshold. From Figure 4b we observe this threshold is $q^* \approx 0.915$, where if $q > q^*$ we see a rapid increase in the trajectory of the system towards $\frac{1}{2}$.

Mathematically characterizing this threshold q^* in terms of graph parameters involves finding a solution to the expressions derived in Theorem 6.5 which has no explicit solution we know of. However, our empirical findings point towards $q^* = \frac{1}{1+\lambda}$.



(a) Deterministic Approximation Φ_t^1 where $\mathbf{P} = \begin{bmatrix} 8 & 10 \\ 10 & 8 \end{bmatrix}$ and (b) Deterministic Approximation Φ_t^2 where $\mathbf{P} = \begin{bmatrix} 10 & 8 \\ 8 & 10 \end{bmatrix}$ and $\mathbf{W} = \begin{bmatrix} 1 & 1 \\ 1 & 1 \end{bmatrix}$.

Figure 3: Plot of two different deterministic approximations Φ_t^1, Φ_t^2 with different \mathbf{P}, \mathbf{W} parameters over $q \in \{0, 0.5, 0.75, 0.95, 1\}$ with $\lambda = 0.1, N_0 = 100$. In Figure 3a, we see $\mu_{RR} < \mu_{RB}$ and $\rho_0 < 1$, so as q increases to 1, our process Φ_t^1 converges to $\frac{1}{2}$ at a slower rate. In Figure 3b, we have $\mu_{RR} > \mu_{RB}$, and $\rho_0 > 1$, so increasing q to 1 has the effect of Φ_t^2 decreasing the rate of convergence to 0.

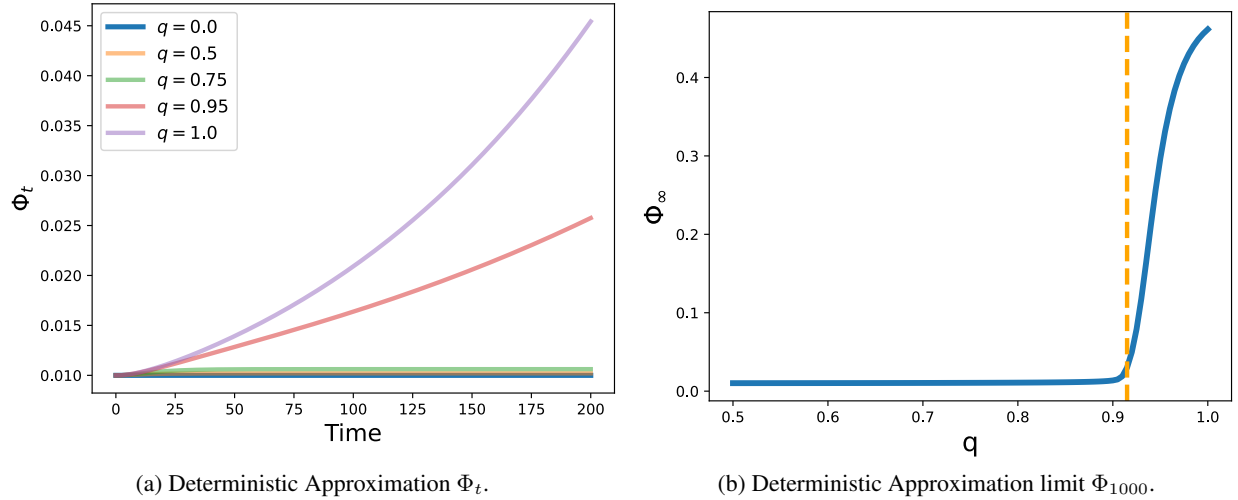


Figure 4: Plot of our deterministic approximation Φ_t and threshold parameter ρ_t for $\mathbf{P} = \begin{bmatrix} 10 & 8 \\ 8 & 10 \end{bmatrix}$ and $\mathbf{W} = \begin{bmatrix} 1 & 1.25 \\ 1.25 & 1 \end{bmatrix}$ over $q \in \{0, 0.5, 0.75, 0.95, 1\}$. Here we see $\mu_{RR} > \mu_{RB}$ and $\rho_0 = 1$, so as q increases, we see our process change from stationary to convergent towards $\frac{1}{2}$. Additionally we plot Φ_{1000} over different values of q . We empirically observe that there is a threshold $q^* \approx 0.915$ where the Φ_{1000} values quickly jump from 0 towards converging to $\frac{1}{2}$.

In Figure 5, the threshold value observed in Figure 4b is plotted over several different λ values in $[0, 1]$. Additionally, the function $f(\lambda) = \frac{1}{1+\lambda}$ is plotted in the dotted line. As the figure shows, the threshold value q^* and $f(\lambda)$ are nearly

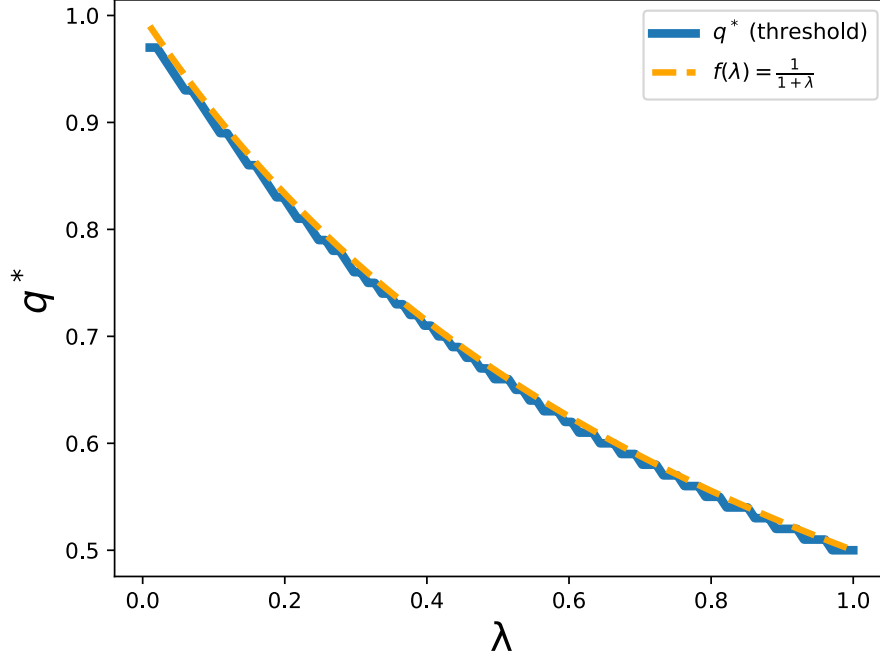


Figure 5: Plot of threshold value q^* of deterministic system over different $\lambda \in [0, 1]$. The dotted orange line is the function $f(\lambda) = \frac{1}{1+\lambda}$. The two lines follow each other almost exactly.

identical (the small deviations in the q^* plot are from discretization when measuring q^*). With this in mind, we propose the following conjecture.

Conjecture 6.5.1. *For any system where $\rho_0 = 1$ and $\mu_{RR} \neq \mu_{RB}$. The following holds for the deterministic approximation Φ_t .*

1. If $q \leq \frac{1}{1+\lambda}$, then $\lim_{t \rightarrow \infty} \Phi_t = \Phi_0$
2. If $q > \frac{1}{1+\lambda}$, then $\lim_{t \rightarrow \infty} \Phi_t = \frac{1}{2}$ if $\mu_{RR} < \mu_{RB}$, and $\lim_{t \rightarrow \infty} \Phi_t = 0$ if $\mu_{RR} > \mu_{RB}$.

From the proof of Lemma 6.1, the condition for convergence of $S_{RR}(t)$ and $S_{RB}(t)$ is $q(1+\lambda) > 1$. Therefore, we hypothesize that if this condition is satisfied, we will have $S_{RR} \propto \mu_{RR}$ and $S_{RB} \propto \mu_{RB}$ thus making $\lim_{t \rightarrow \infty} \rho_t \approx \frac{\mu_{RR}}{\mu_{RB}}$, allowing convergence to be determined according to Theorem 6.5.

7 APS Dataset & Model Validation

To validate this model, we assess gender diversity in scientific collaboration networks. We use the co-authorship network from the American Physical Society (APS) [1], a database of Physics publications that has been used on a variety of meta-analyses of research collaborations [31, 45]. In particular, we use a filtered version of the data set as in [45]. We join this with the citation data from [1]. We use this network to find how often a paper is cited within the APS community, which serves as a proxy for edge weight in our model.

7.1 APS Dataset Information

7.1.1 Data Processing

We largely follow the procedure used in [31]. First, we used data provided in [45] which de-duplicates author names. We also restrict all publications to those that have been published between 1980 and 2009. The primary reason for this is because [45] provides a supplementary dataset of publications with the de-duplicated author names from 1893 until 2010, and to control for large political changes, we only selected the final three decades. We also exclude the year

2010 because the supplementary data in [45] did not provide data for the full year of 2010. We also only include *active authors*, defined as authors who have, since their first publication, published at least once every five years until the most recent year 2009. Additionally, we filtered the data by removing all publications with 0 authors.

To predict the gender of authors, we used the pre-trained gender classifier GenderPerformr [49]. We let GenderPerformr predict gender for our authors in the dataset and only kept the authors whose gender could be predicted with $> 80\%$ confidence. We note that this model could potentially be biased towards Western-sounding names, which could reduce the relevance of our analysis as applied to diversity in Physics collaborations. We also note that this model classifies gender on a Male/Female binary, which does not accurately reflect all authors' gender identities.

This left us with a set of 14,793 authors, which formed our collaboration network. We consider our collaboration network as a sequence of graphs over time, $G_t = (V_t, E_t)$ where $t \in \{1980, \dots, 2009\}$. For time t , our nodes V_t are the set of authors whose first publication was *at or before* time t . This formulation ensures that our network will constantly grow over time. A pair of nodes is connected with an edge if the two nodes co-authored a paper together. In the case of a paper having more than two authors, we default to connecting the first and last authors of the paper, following the procedure in [31]. However, in the case that the first or last co-author is either a non-active author or their gender couldn't be predicted by GenderPerformr, we choose the authors nearest to the first/last position (i.e. if the first author isn't available, choose the second author, same with last and second to last authors and so on). This procedure alters the data by removing all author-publication pairs if the author was not nearest to the first or last (i.e. if Author A wrote one paper in 1980 where they were the third author out of seven, they would not appear in the graph for 1980, but instead would appear whenever they were nearest to first/last author of a paper). We allow for self-edges if the author published a paper with no co-authors. Each edge is given weight according to the number of citations received five years after the paper has been published. The best-fit model to the data according to this edge generation is shown in Figure 1.

An alternate strategy for creating a collaboration network is to connect all pairs of coauthors on a paper. However, this leads to an over-representation of papers with large numbers of co-authors in our weight computation, and reduces our model's predictive accuracy, as seen in Figure 6.

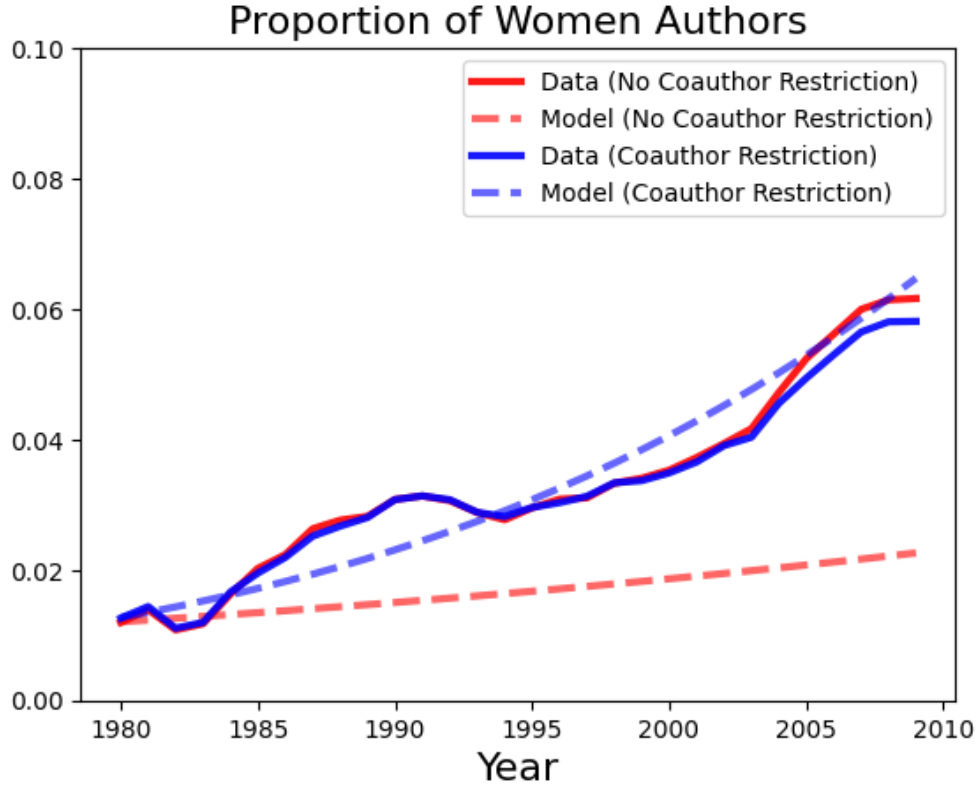


Figure 6: Plot of the proportion of women in the APS co-authorship network from 1980-2009 for data created with no restriction on coauthorship (every pair of coauthors is connected in the graph) in red, and data created where only the first and last authors connected (approximately, see text for exact procedure) in blue. The deterministic model's predictions are overlaid in the dashed lines.

7.2 Estimating Model Parameters

To fit our model to the data, we perform the following procedure to estimate model parameters. We assume our probability and weight matrices at time t are of the form $\mathbf{P}_t = \begin{bmatrix} \mu_{MM}(t) & \mu_{MF}(t) \\ \mu_{MF}(t) & \mu_{FF}(t) \end{bmatrix}$, $\mathbf{W}_t = \begin{bmatrix} w_{MM}(t) & w_{MF}(t) \\ w_{MF}(t) & w_{FF}(t) \end{bmatrix}$, meaning subscripts MM and MF represent *in-community* and *cross-community* parameters respectively. To estimate our in-community probability parameter $\hat{\mu}_{MM}(t)$, we counted all in-community edges (both $M - M$ and $F - F$) and divided them by the total number of possible in-community edges in our Graph. Let $n_{MM}(t)$, $n_{MF}(t)$, $n_{FF}(t)$ be the number of Male-Male, Male-Female, and Female-Female edges present in our collaboration network G_t , respectively. Then our estimated parameter can be defined as

$$\hat{\mu}_{MM}(t) = n_t \left(\frac{n_{MM}(t) + n_{FF}(t)}{(n_t^M)^2 + (n_t^F)^2} \right). \quad (26)$$

$\hat{\mu}_{MF}(t)$ is computed similarly. To derive our in-community weight parameter $\hat{w}_{MM}(t)$ (or similarly $\hat{w}_{MF}(t)$), we averaged the weights over all in-community edges at time t .

$$\hat{w}_{MM}(t) = \frac{\sum_{c[i], c[j] \in (M, M), (F, F)} (w_{ij})_t}{n_{MM}(t) + n_{FF}(t)}. \quad (27)$$

To derive the probability of an edge persisting from time t to time $t + 1$, we consider the set $E_t \cap E_{t+1}$, which is the set of edges present in both G_t and G_{t+1} and find their ratio with respect the number of edges in G_t as

$$\hat{q}_t = \frac{|E_t \cap E_{t+1}|}{|E_t|}. \quad (28)$$

Finally, to estimate the network growth parameters, we perform an exponential curve-fitting on the size of the network over time. Namely, choose approximation $f(t) := \tilde{N}_0(1 + \hat{\lambda})^t$ which minimizes L_2 error over our network size $|V_t|$. Formally, we have

$$\hat{\lambda}, \hat{N}_0 = \arg \min_{\lambda, N_0} \sum_{t=1980}^{2009} (N_0(1 + \lambda)^t - |V_t|)^2. \quad (29)$$

In order to find the overall estimates $\hat{\mathbf{P}}, \hat{\mathbf{W}}, \hat{q}$, we simply average over times t , which results in $\hat{\mathbf{P}} = \begin{bmatrix} 0.359 & 0.468 \\ 0.468 & 0.359 \end{bmatrix}$, $\hat{\mathbf{W}} = \begin{bmatrix} 14.337 & 18.026 \\ 18.026 & 14.337 \end{bmatrix}$, $\hat{q} = 0.265$, $\hat{\lambda} = 0.115$, $\hat{N}_0 = 466.2$ being the estimated parameters for our model with coauthor restriction. For the model in Figure 6 with no coauthor restriction, these estimated parameters were $\hat{\mathbf{P}} = \begin{bmatrix} 0.511 & 0.718 \\ 0.718 & 0.511 \end{bmatrix}$, $\hat{\mathbf{W}} = \begin{bmatrix} 54.71 & 47.17 \\ 47.17 & 54.71 \end{bmatrix}$, $\hat{q} = 0.309$, $\hat{\lambda} = 0.116$, $\hat{N}_0 = 473.0$. Note that we do not use \hat{N}_0 in generating any of the plots. Instead, we use the true value of $N_0 = 251$.

7.3 Results & Discussion

With the optimal estimated parameter values from Section 7.2, we fit the model to our dataset and assessed how accurately the model predicts the growth of women authors in the scientific collaboration network, as in Figure 1. In the data, we see that from 1980-2009, the proportion of active women researchers grew from around 1% to 6%. This is roughly captured by our model when fitted to the dataset, predicting slightly over 6% active women researchers in 2009. We also observe that the addition of memory did not significantly change the model's predicted trajectory. The estimated parameters from Section 7.2 suggest that increasing q will cause a slower rate of convergence to $\frac{1}{2}$. However, we empirically observe that the estimated memory parameter $\hat{q} = 0.265$ does not meaningfully alter the trajectory when compared to the no memory case of $q = 0$. This was suggested by Figures 3 & 4, since in those figures large shifts away from the baseline trajectory occurred only after q was close to 1.

These results show that a combination of node influence (through preferential attachment) and homophily can partially explain the growth of the minority population in a scientific collaboration network. This result offers a powerful tool for understanding the impact of network dynamics on diversity in scientific communities, though some finer-tuned analysis is necessary to make it more accurate for prediction.

8 Model Extensions

8.1 "Soft" Homophily

To introduce soft homophily to our model, we define parameter $\alpha \in [0, 1]$ which is the probability that a node will recruit another node with a different color. For example, a model with $\alpha = 0$ is the same base model as in Section 4, $\alpha = 0.5$ is a model where nodes will recruit colors at random, and $\alpha = 1$ is *heterophily*, where recruitment happens in the opposite direction as the base model ("like recruits unlike"). To assess the effect α has on the stochastic process, we create $n = 10$ trajectories for each $\alpha \in \{0, 0.25, 0.5, 0.75, 1\}$, and plot the mean trajectory along with confidence bands. We repeat this for two parameter values, $\mathbf{P} = \begin{bmatrix} 10 & 20 \\ 20 & 10 \end{bmatrix}$, $\mathbf{W} = \begin{bmatrix} 1 & 1.25 \\ 1.25 & 1 \end{bmatrix}$ (base model converges to $\frac{1}{2}$) and $\mathbf{P} = \begin{bmatrix} 10 & 8 \\ 8 & 10 \end{bmatrix}$, $\mathbf{W} = \begin{bmatrix} 1 & 1 \\ 1 & 1 \end{bmatrix}$ (base model converges to 0).

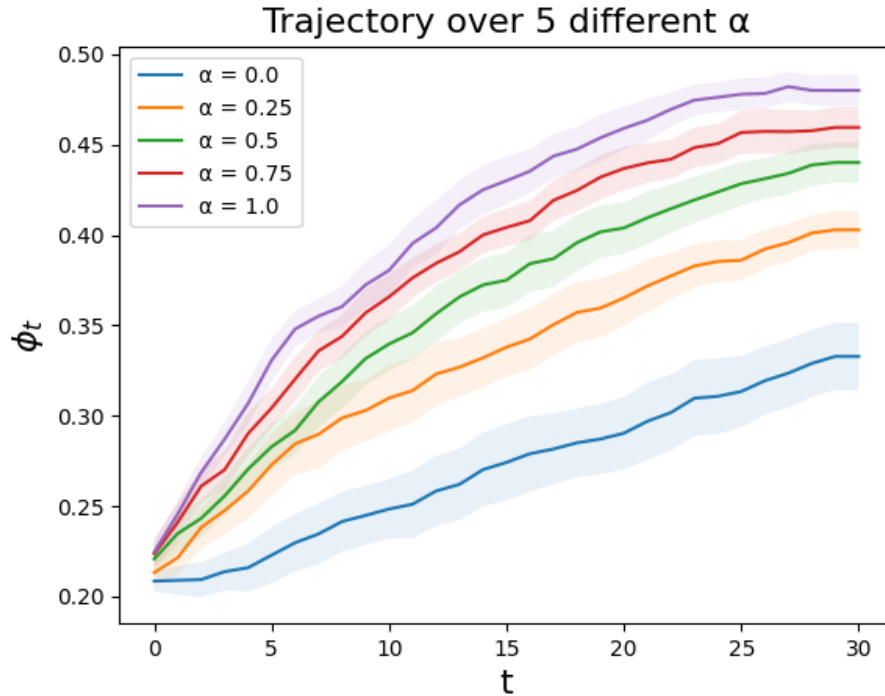


Figure 7: Mean trajectories of ϕ_t over $\alpha \in \{0, 0.25, 0.5, 0.75, 1\}$ with confidence bands. $\mathbf{P} = \begin{bmatrix} 10 & 20 \\ 20 & 10 \end{bmatrix}$, $\mathbf{W} = \begin{bmatrix} 1 & 1.25 \\ 1.25 & 1 \end{bmatrix}$. The base system ($\alpha = 0$) converges to $\frac{1}{2}$, and as α increases, we see the system converges to $\frac{1}{2}$ faster

From Figures 7 and 8, we can see that as $\alpha \rightarrow 1$ and homophily in recruiting decreases, our system begins to converge to $\frac{1}{2}$. The rate of this convergence also seems to scale with the value of α , where higher α leads to faster convergence. We find this shift is independent of the convergence of the base system ($\alpha = 0$). In Figure 7, the base system converges to $\frac{1}{2}$, and increasing α accelerates this convergence. However, in Figure 8, the base system converges to 0, but an increase in α still changes the convergence of the system to $\frac{1}{2}$. We can mathematically support these observations by proving that in expectation, the proportion of minority nodes is non-decreasing in α .

Lemma 8.1. *For all t , we have $\mathbb{E} \left[\frac{R_t}{R_t + B_t} \right] \leq \frac{1}{2}$.*

Proof. We want to show $\mathbb{E} \left[\frac{R_t}{R_t + B_t} \right] \leq \mathbb{E} \left[\frac{B_t}{R_t + B_t} \right]$. Define RR_t, RB_t, BB_t as the number of Red-Red, Red-Blue, and Blue-Blue edges at time t . These are all binomial random variables, with $RR_t \sim \text{Bin} \left(\frac{1}{2}(n_t^R)^2, \frac{\mu_{RR}}{n_t} \right)$, $RB_t \sim$

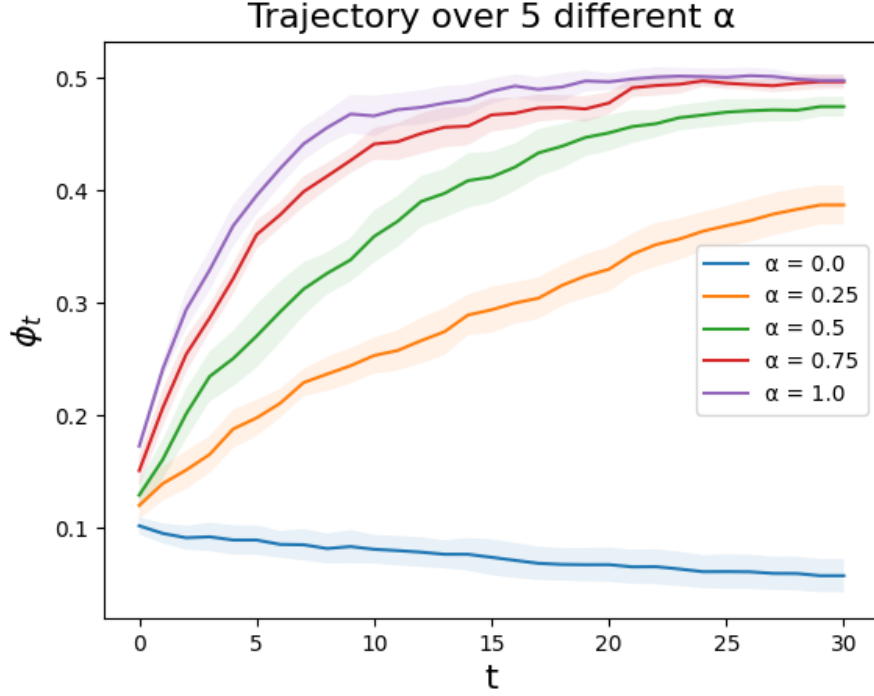


Figure 8: Mean trajectories of ϕ_t over $\alpha \in \{0, 0.25, 0.5, 0.75, 1\}$ with confidence bands. $\mathbf{P} = \begin{bmatrix} 10 & 8 \\ 8 & 10 \end{bmatrix}$, $\mathbf{W} = \begin{bmatrix} 1 & 1 \\ 1 & 1 \end{bmatrix}$. The base system ($\alpha = 0$) converges to 0, but as α increases, we see the convergence of the system change to converge to $\frac{1}{2}$

$\text{Bin}\left(n_t^R n_t^B, \frac{\mu_{RB}}{n_t}\right)$ and $BB_t \sim \text{Bin}\left(\frac{1}{2}(n_t^B)^2, \frac{\mu_{RR}}{n_t}\right)$. Because Red is the minority, we have $n_t^R \leq n_t^B$, so we can define $BB_t := Y_t + Z_t$, where $Y_t \sim \text{Bin}\left(\frac{1}{2}(n_t^R)^2, \frac{\mu_{RR}}{n_t}\right)$, and $Z_t \sim \text{Bin}\left(\frac{1}{2}((n_t^B)^2 - (n_t^R)^2), \frac{\mu_{RR}}{n_t}\right)$. Since $RR_t \sim Y_t$, we know $\mathbb{E}\left[\frac{RR_t}{R_t + B_t}\right] = \mathbb{E}\left[\frac{Y_t}{R_t + B_t}\right]$. We now simplify our expression as follows:

$$\mathbb{E}\left[\frac{B_t}{R_t + B_t}\right] = \mathbb{E}\left[\frac{BB_t + RB_t}{R_t + B_t}\right] \quad (30)$$

$$= \mathbb{E}\left[\frac{Y_t}{R_t + B_t}\right] + \mathbb{E}\left[\frac{Z_t}{R_t + B_t}\right] + \mathbb{E}\left[\frac{RB_t}{R_t + B_t}\right] \quad (31)$$

$$= \mathbb{E}\left[\frac{RR_t}{R_t + B_t}\right] + \mathbb{E}\left[\frac{Z_t}{R_t + B_t}\right] + \mathbb{E}\left[\frac{RB_t}{R_t + B_t}\right] \quad (32)$$

$$\geq \mathbb{E}\left[\frac{RR_t}{R_t + B_t}\right] + \mathbb{E}\left[\frac{RB_t}{R_t + B_t}\right] \quad (33)$$

$$= \mathbb{E}\left[\frac{R_t}{R_t + B_t}\right]. \quad (34)$$

Therefore we have $\mathbb{E}\left[\frac{R_t}{R_t + B_t}\right] \leq \mathbb{E}\left[\frac{B_t}{R_t + B_t}\right]$, and since $\mathbb{E}\left[\frac{R_t}{R_t + B_t}\right] + \mathbb{E}\left[\frac{B_t}{R_t + B_t}\right] = 1$, we know $\mathbb{E}\left[\frac{R_t}{R_t + B_t}\right] \leq \frac{1}{2}$, completing the proof. \square

Theorem 8.2. $\mathbb{E}[\phi_\alpha(t)]$ is non-decreasing in α . If $\alpha_1 \leq \alpha_2$, then $\mathbb{E}[\phi_{\alpha_1}(t)] \leq \mathbb{E}[\phi_{\alpha_2}(t)]$ for all $t \geq 0$.

Proof. We prove this by induction. Define $\Phi_\alpha(t) := \mathbb{E}[\phi_\alpha]$. For $t = 0$, we have $\phi_\alpha(0) = \frac{N_0^R}{n_0}$ for all α .

For the inductive step, assume $\Phi_{\alpha_1}(t) \leq \Phi_{\alpha_2}(t)$ for $\alpha_1 \leq \alpha_2$. Define $m_{t+1} := \lambda n_t$ as the number of new nodes that arrive in time $t + 1$. We will derive the probability a New node is red in terms of α . Consider a new node i , Let $r[i] \in \{R, B\}$ equal the statement *node i was recruited by a Red/Blue node*.

$$P(c[i] = R) = P(c[i] = R | r[i] = R)P(r[i] = R) \quad (35)$$

$$+ P(c[i] = R | r[i] = B)P(r[i] = B) \quad (36)$$

$$= (1 - \alpha) \left(\frac{R_t}{R_t + B_t} \right) + \alpha \left(\frac{B_t}{R_t + B_t} \right) \quad (37)$$

$$= \left(\frac{1}{R_t + B_t} \right) ((1 - \alpha)R_t + \alpha B_t). \quad (38)$$

We use this probability to find the relationships between $\mathbb{E}[N_t^R]$ and $\mathbb{E}[N_{t+1}^R]$.

$$\mathbb{E}[N_{t+1}^R | N_t^R] = N_t^R + m_{t+1} P(c[i] = R) \quad (39)$$

$$= N_t^R + m_{t+1} \left((1 - \alpha) \left(\frac{R_t}{R_t + B_t} \right) + \alpha \left(\frac{B_t}{R_t + B_t} \right) \right) \quad (40)$$

$$\mathbb{E}[\mathbb{E}[N_{t+1}^R | N_t^R]] = \mathbb{E}[N_t^R] + \lambda n_t \left((1 - \alpha) \mathbb{E} \left[\frac{R_t}{R_t + B_t} \right] + \alpha \mathbb{E} \left[\frac{B_t}{R_t + B_t} \right] \right) \quad (41)$$

$$n_{t+1} \Phi_\alpha(t + 1) = n_t \Phi_\alpha(t) + \lambda n_t \left((1 - \alpha) \mathbb{E} \left[\frac{R_t}{R_t + B_t} \right] + \alpha \mathbb{E} \left[\frac{B_t}{R_t + B_t} \right] \right) (1 + \lambda) \Phi_\alpha(t + 1) \quad (42)$$

$$= \Phi_\alpha(t) + \lambda \cdot \left(\mathbb{E} \left[\frac{R_t}{R_t + B_t} \right] + \alpha \left(1 - 2 \mathbb{E} \left[\frac{R_t}{R_t + B_t} \right] \right) \right) \quad (43)$$

$$\Phi_\alpha(t + 1) = \left(\frac{1}{1 + \lambda} \right) (\Phi_\alpha(t)) + \left(\frac{\lambda}{1 + \lambda} \right) \left(\mathbb{E} \left[\frac{R_t}{R_t + B_t} \right] + \alpha \left(1 - 2 \mathbb{E} \left[\frac{R_t}{R_t + B_t} \right] \right) \right). \quad (44)$$

Since we have shown $\mathbb{E} \left[\frac{R_t}{R_t + B_t} \right] \leq \frac{1}{2}$ in Lemma 8.1, we see that $\Phi_\alpha(t + 1)$ is linear in α with slope $1 - 2 \mathbb{E} \left[\frac{R_t}{R_t + B_t} \right] \geq 0$. Therefore for $\alpha_1 \leq \alpha_2$ and $\Phi_{\alpha_1}(t) \leq \Phi_{\alpha_2}(t)$, we see that $\Phi_{\alpha_1}(t + 1) \leq \Phi_{\alpha_2}(t + 1)$, completing the proof. \square

The natural next question is understanding at what α values significant changes in convergence occur. Visualizing the α landscape in this way could help identify potential threshold values where slight perturbations cause rapid changes in convergence. We proceed with the same model parameters as in Figure 8, with $\mathbf{P} = \begin{bmatrix} 10 & 8 \\ 8 & 10 \end{bmatrix}$, and $\mathbf{W} = \begin{bmatrix} 1 & 1 \\ 1 & 1 \end{bmatrix}$.

Note that the base model with these parameters converges to 0, whereas the same parameters with $\alpha = 1$ converges to $\frac{1}{2}$. For each $\alpha \in \{0, 0.02, 0.04, \dots, 0.98, 1\}$ we generate $n = 10$ trajectories of length $T = 30$ from our stochastic simulation, and take the final value ϕ_{30} from each one. With these final values for each alpha, we plot the mean and confidence bands across all α to create a plot of ϕ_{30} with respect to α .

As we can see from Figure 9 as α increases, we see an increase in the values of ϕ_{30} , showing the system that converges to 0 when $\alpha = 0$ changes to converge to $\frac{1}{2}$ when α increases to 1. We also observe the absence of a threshold value where change occurs rapidly in convergence. Instead, we observe a steady increase in the value of ϕ_{30} . Additionally, more theoretical work must be done to assess the limiting value of ϕ_∞ , so we can understand the convergent behavior of the system where the empirical results are less clear (for example, $\alpha = 0.01$).

8.2 Node Departures

With the addition of departures, nodes can both join the network ("recruitment") and leave the network ("retirement"). To amend our model to include node departures, we define parameter $\eta \in [0, 1]$ that represents the *departure rate* of nodes in the graph. Graph departures take place *after* the recruitment step and *before* the creation of the next graph.

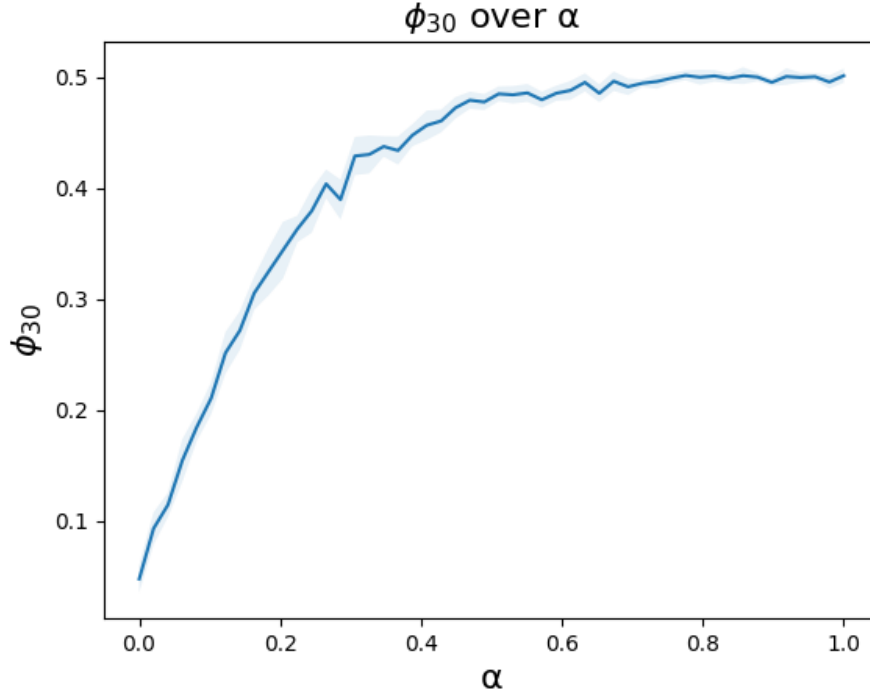


Figure 9: Plot of mean trajectory and confidence bands of ϕ_{30} over α , with $\mathbf{P} = \begin{bmatrix} 10 & 10 \\ 10 & 10 \end{bmatrix}$, $\mathbf{W} = \begin{bmatrix} 1.5 & 1 \\ 1 & 1.5 \end{bmatrix}$. The base system ($\alpha = 0$) converges to 0, and we see as α increases the value ϕ_{30} steadily increases, until we see $\phi_{30} = \frac{1}{2}$ for $\alpha = 1$

Nodes depart from a graph according to what we define as "inverse preferential attachment". For recruitment, Red nodes join the graph at rate proportional to the "success" of Red nodes already in the graph. Likewise, for retirement Red nodes leave the graph at a rate *inversely proportional* to the "success" of Red nodes in the graph. For example, if Red nodes have low total weight in their collaborations, then more Red nodes will depart from the graph compared to if red nodes had higher weighted degrees.

We define our updated graph dynamics with node departures included.

Definition 8.3 (Stochastic Block Model Dynamics with Departures). *Let $G_t = (V_t, E_t)$ be our graph at time t . Assume this graph contains n_t nodes, with n_t^R Red nodes and n_t^B Blue nodes. Our procedure for generating the subsequent graph G_{t+1} is as follows:*

1. Calculate the total weight of Red nodes and Blue nodes in G_t , defined as $R_t = \sum_{c[i]=R} \sum_{j \in [n_t]} w_{ij}$, and $B_t = \sum_{c[i]=B} \sum_{j \in [n_t]} w_{ij}$.
2. Define intermediate graph $G_t^+ = (V_t, E_t^+)$ where for every edge $(i, j) \in E_t$, with probability q let $(i, j) \in E_t^+$, otherwise remove it.
3. Add $m_{t+1} := \lceil \lambda n_t \rceil$ new nodes to graph G_t^+ . Each incoming node is Red with probability $\frac{R_t}{R_t + B_t}$, or Blue with probability $\frac{B_t}{R_t + B_t}$.
4. For every red node i in G_t , node i departs graph G_t^+ with probability $\omega_R := \eta \left(\frac{B_t}{R_t + B_t} \right)$ and for blue nodes in G_t , departs with probability $\omega_B := \eta \left(\frac{R_t}{R_t + B_t} \right)$.
5. Initialize $G_{t+1} = G_t^+$, and for all potential edges $(i, j) \notin E_t^+$, generate them according the Weighted Stochastic Block Model with parameters \mathbf{P} and \mathbf{W} .

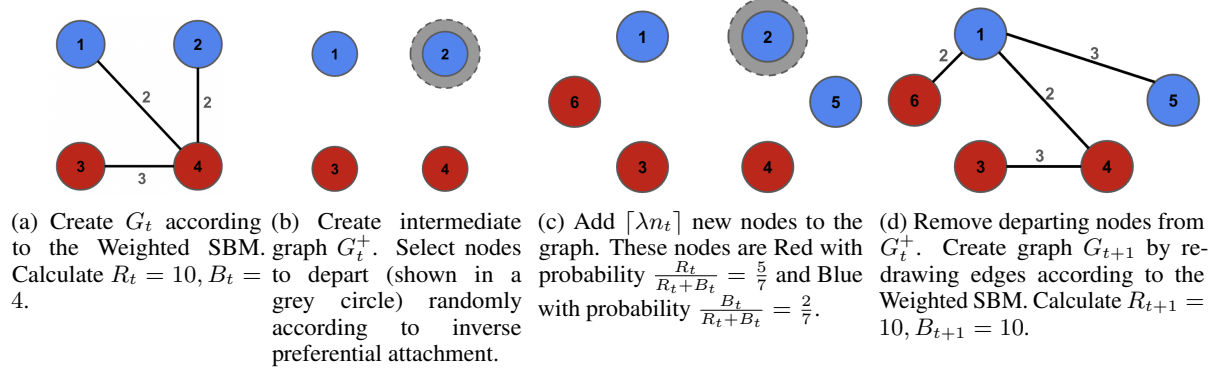


Figure 10: Visualization of the Stochastic Block Model Dynamics with departures described in Definition 8.3 for $\mathbf{P} = \begin{bmatrix} 0.7 & 1 \\ 1 & 0.7 \end{bmatrix}$, $\mathbf{W} = \begin{bmatrix} 3 & 2 \\ 2 & 3 \end{bmatrix}$, $\lambda = 0.5$, and $\eta = 0.5$. Figure 10a shows initialization of G_t . Figure 10b shows the intermediate graph G_t^+ with departing nodes randomly selected according to preferential attachment and departure parameter η . Figure 10c shows new nodes being added to the network according to preferential attachment, and Figure 10d shows the departing nodes leaving the graph, and the creation of G_{t+1} according to the Weighted SBM from Definition 4.1

This definition is illustrated in Figure 10. In this model, not only are minority nodes less likely to join a graph where similar nodes have less success, but they are also more likely to leave.

To analyze how the η parameter changes the convergence of the minority proportion ϕ_t , we simulate $n = 20$ trajectories and plot the mean trajectories over $\eta \in \{0, 0.25, 0.5, 0.75, 1\}$.

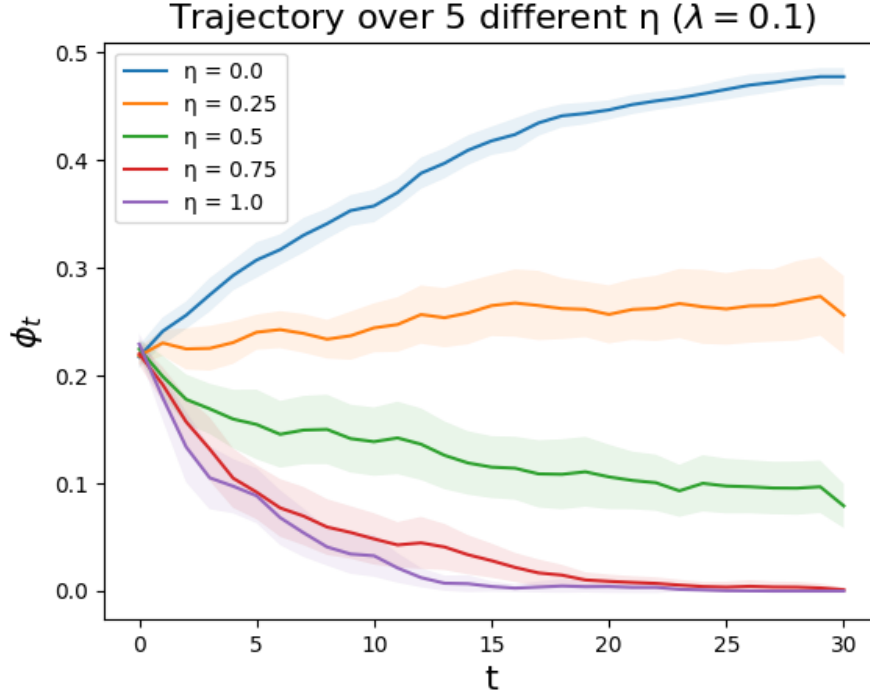


Figure 11: Plot of mean trajectory with confidence bands ($n=20$) over $\eta \in \{0, 0.25, 0.5, 0.75, 1\}$ for model with parameters $\mathbf{P} = \begin{bmatrix} 10 & 1 \\ 1 & 10 \end{bmatrix}$, $\mathbf{W} = \begin{bmatrix} 1 & 1 \\ 1 & 1 \end{bmatrix}$, and arrival rate $\lambda = 0.1$. For $\eta = 0$, we see the system converges to $\frac{1}{2}$. As η goes to 1, the trajectory of the system changes to static and ultimately changes to converge to 0.

From Figure 11 we see that an increase in the departure rate η causes a decrease in the trajectories of the system. In the base system ($\eta = 0$), we have $\rho_0 = 0.1$, indicating convergence to $\frac{1}{2}$. When $\eta = 0.25$, we see the trajectory flatten, suggesting a static equilibrium. Furthermore, as η increases towards 1, we see the convergence of the system switch, instead heading towards 0 where the minority vanishes.

To see how increasing η affects the convergence of the system, we plot the values of ϕ_{30} for the same system as Figure 11 over $\eta \in [0, 1]$. From Figure 12, we see as η increases, ϕ_{30} steadily decreasing. We also notice that at high values of

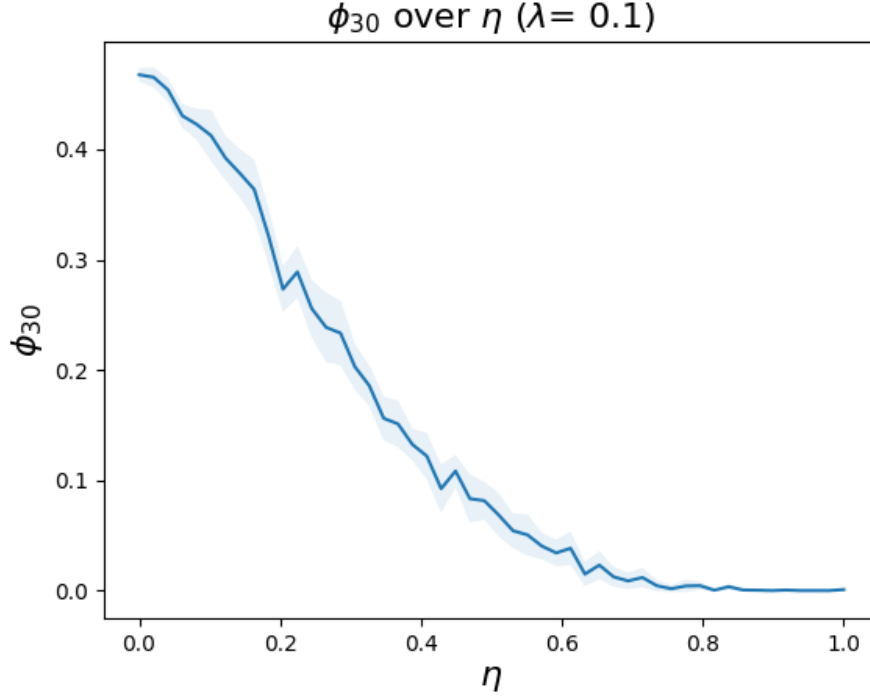


Figure 12: Plot of mean ϕ_{30} over $\eta \in [0, 1]$ with confidence bands. The parameters for the system are $\mathbf{P} = \begin{bmatrix} 10 & 1 \\ 1 & 10 \end{bmatrix}$, $\mathbf{W} = \begin{bmatrix} 1 & 1 \\ 1 & 1 \end{bmatrix}$, and arrival rate $\lambda = 0.1$. As η increases, we see a smooth decrease of the ϕ_{30} value, changing from near $\frac{1}{2}$ for $\eta = 0$ to near 0 for $\eta = 1$.

η , the value of ϕ_{30} becomes 0 with very high confidence. In the base model, the minority "vanishes" from the graph as $\phi_t \rightarrow 0$. However, in the model with departures, it is possible for $\phi_t = 0$, meaning all minority nodes have left the graph, leaving only one community.

9 Conclusion

The above model is a simple abstraction that captures the effect of homophily in networks on long-term diversity, which matches sociological observations of workplace diversity and networks with preferential attachment [43, 27, 42]. Many other factors must be considered before we can have an end-to-end model, from pre-recruitment to promotion, and this is a clear limitation of our work. To expand the model we could look at node creation mechanisms beyond preferential attachment, such as a constant number of new nodes joining each timestep, or a time-inhomogenous rate parameter λ_t , to model seasonality trends in the recruitment step. This model is also hindered by the fact that it only has fixed points of $\{0, \frac{1}{2}, 1\}$ when in actuality, diversity isn't usually judged by equivalent parity, but rather representative parity. Finding ways to mathematically extend the model to arbitrary fixed points would be an important future step.

A possible future research direction could be an assessment of policies that are purported to increase diversity with our model. Such analyses could reveal whether these policies fully anticipated the dynamics of networks as having a significant impact on long-term diversity. This could provide a significant intervention in academic and professional recruitment "best practices".

With this in mind, our model and our findings about its threshold property could point towards a network analysis of institutions to establish whether cross-community collaborations are frequent enough or weighted highly enough to encourage lasting diversity. This is a powerful tool because an organization can look at how a network is at one point in time, and use it to extrapolate into the future, as well as develop interventions for the present (e.g. incentives to encourage more cross-community collaborations).

References

- [1] APS Data Sets for Research — journals.aps.org. <https://journals.aps.org/datasets>. [Accessed 24-02-2024].
- [2] Joan Acker. Inequality regimes: Gender, class, and race in organizations. *Gender and Society*, 20(4):441–464, 2006.
- [3] Christopher Aicher, Abigail Z Jacobs, and Aaron Clauset. Adapting the stochastic block model to edge-weighted networks. *arXiv preprint arXiv:1305.5782*, 2013.
- [4] Christopher Aicher, Abigail Z. Jacobs, and Aaron Clauset. Learning latent block structure in weighted networks. *Journal of Complex Networks*, 3(2):221–248, June 2014.
- [5] Lauren M. Alfrey. Diversity, Disrupted: A Critique of Neoliberal Difference in Tech Organizations. *Sociological Perspectives*, 65(6):1081–1098, December 2022. Publisher: SAGE Publications Inc.
- [6] Mackenzie Alston. Eliminating discrimination in hiring isn't enough. *IZA World of Labor*, 2023.
- [7] Lars Backstrom, Dan Huttenlocher, Jon Kleinberg, and Xiangyang Lan. Group formation in large social networks: membership, growth, and evolution. In *Proceedings of the 12th ACM SIGKDD international conference on Knowledge discovery and data mining*, pages 44–54, 2006.
- [8] Albert-László Barabási and Réka Albert. Emergence of scaling in random networks. *science*, 286(5439):509–512, 1999.
- [9] Albert-Laszlo Barabási, Hawoong Jeong, Zoltan Nédá, Erzsebet Ravasz, Andras Schubert, and Tamas Vicsek. Evolution of the social network of scientific collaborations. *Physica A: Statistical mechanics and its applications*, 311(3-4):590–614, 2002.
- [10] Marianne Bertrand and Sendhil Mullainathan. Are Emily and Greg More Employable Than Lakisha and Jamal? A Field Experiment on Labor Market Discrimination. *American Economic Review*, 94(4):991–1013, September 2004.
- [11] Simina Brânzei, Nithish Kumar, and Gireeja Ranade. Phase transitions of diversity in stochastic block model dynamics. In *2023 59th Annual Allerton Conference on Communication, Control, and Computing (Allerton)*, pages 1–8. IEEE, 2023.
- [12] Ronald S. Burt. Structural Holes and Good Ideas. *American Journal of Sociology*, 110(2):349–399, 2004. Publisher: The University of Chicago Press.
- [13] Antoni Calvo-Armengol and Yannis M. Ioannides. Social Networks in Labor Markets. Discussion Papers Series, Department of Economics, Tufts University 0517, Department of Economics, Tufts University, 2005.
- [14] Antoni Calvo-Armengol, Eleonora Patacchini, and Yves Zenou. Peer effects and social networks in education. *The Review of Economic Studies*, 76(4):1239–1267, 2009.
- [15] Kenneth A. Couch, Joni Hersch, and Jennifer Bennett Shinall. Fifty years later: The legacy of the civil rights act of 1964. *Journal of Policy Analysis and Management*, 34(2):424–456, 2015.
- [16] T. Cox. *Cultural Diversity in Organizations: Theory, Research and Practice*. Berrett-Koehler Publishers, 1993.
- [17] Matthew Eichhorn, Siddhartha Banerjee, and David Kempe. Online team formation under different synergies. In *Workshop on Internet and Network Economics*, 2022.
- [18] Mark S. Granovetter. The Strength of Weak Ties. *American Journal of Sociology*, 78(6):1360–1380, 1973. Publisher: University of Chicago Press.
- [19] Peter Grindrod and Mark Parsons. Social networks: Evolving graphs with memory dependent edges. *Physica A: Statistical Mechanics and its Applications*, 390(21-22):3970–3981, 2011.
- [20] Cedric Herring and Loren Henderson. From affirmative action to diversity: Toward a critical diversity perspective. *Critical Sociology*, 38(5):629–643, 2012.
- [21] Paul W. Holland, Kathryn Blackmond Laskey, and Samuel Leinhardt. Stochastic blockmodels: First steps. *Social Networks*, 5(2):109–137, 1983.

- [22] Lu Hong and Scott E. Page. Groups of diverse problem solvers can outperform groups of high-ability problem solvers. *Proceedings of the National Academy of Sciences*, 101(46):16385–16389, 2004.
- [23] Jian Huang, Ziming Zhuang, Jia Li, and C Lee Giles. Collaboration over time: characterizing and modeling network evolution. In *WSDM*, pages 107–116, 2008.
- [24] Matthew O Jackson and Asher Wolinsky. A strategic model of social and economic networks. In *Networks and groups*, pages 23–49. Springer, 2003.
- [25] Jamie Dolkas Joan C. Williams. Data-Driven Diversity — hbr.org. <https://hbr.org/2022/03/data-driven-diversity>. [Accessed 26-01-2024].
- [26] Judd Kessler and Corinne Low. Research: How Companies Committed to Diverse Hiring Still Fail — hbr.org. <https://hbr.org/2021/02/research-how-companies-committed-to-diverse-hiring-still-fail>. [Accessed 16-01-2024].
- [27] Kibae Kim and Jörn Altmann. Effect of homophily on network formation. *Communications in Nonlinear Science and Numerical Simulation*, 44:482–494, March 2017.
- [28] Jon Kleinberg, Sendhil Mullainathan, and Manish Raghavan. Inherent trade-offs in the fair determination of risk scores. In *ITCS*, 2016.
- [29] Oliver Knill. Probability theory and stochastic processes with applications. <https://people.math.harvard.edu/~knill/books/KnillProbability.pdf>. 2009. [Accessed 23-02-2024].
- [30] Clement Lee and Darren J. Wilkinson. A review of stochastic block models and extensions for graph clustering. *Applied Network Science*, 4(1), December 2019.
- [31] Weihua Li, Tomaso Aste, Fabio Caccioli, and Giacomo Livan. Early coauthorship with top scientists predicts success in academic careers. *Nature Communications*, 10:5170, November 2019.
- [32] Stephanie Lunn and Monique Ross. Cracks in the foundation: Issues with diversity and the hiring process in computing fields, 2021.
- [33] Miller McPherson. An ecology of affiliation. *American Sociological Review*, 48(4):519–532, 1983.
- [34] Miller McPherson, Lynn Smith-Lovin, and James M. Cook. Birds of a feather: Homophily in social networks. *Annual Review of Sociology*, 27:415–444, 2001.
- [35] Francisco Bauzá Minguez, Mario Floría, Jesús Gómez-Gardeñes, Alex Arenas, and Alessio Cardillo. Characterization of interactions' persistence in time-varying networks - Scientific Reports — nature.com. <https://www.nature.com/articles/s41598-022-25907-7#citeas>. [Accessed 21-01-2024].
- [36] Shira Mitchell, Eric Potash, Solon Barocas, Alexander D'Amour, and Kristian Lum. Algorithmic fairness: Choices, assumptions, and definitions. *Annual Review of Statistics and Its Application*, 8:141–163, 2021.
- [37] Pamela Newkirk. *Diversity, Inc.: The Failed Promise of a Billion-Dollar Business*. Bold Type Books, New York, October 2019.
- [38] Tiago P. Peixoto. Nonparametric weighted stochastic block models. *Phys. Rev. E*, 97:012306, January 2018.
- [39] Andi Peng, Besmira Nushi, Emre Kıcıman, Kori Inkpen, Siddharth Suri, and Ece Kamar. What You See Is What You Get? The Impact of Representation Criteria on Human Bias in Hiring. *Proceedings of the AAAI Conference on Human Computation and Crowdsourcing*, 7:125–134, October 2019.
- [40] S. S. Phulari, S. D. Khamitkar, N. K. Deshmukh, P. U. Bhalchandra, S. N. Lokhande, and A. R. Shinde. Understanding Formulation of Social Capital in Online Social Network Sites (SNS), February 2010.
- [41] Fereshteh Rabbani, Tamer Khraisha, Fatemeh Abbasi, and Gholam Reza Jafari. Memory effects on link formation in temporal networks: A fractional calculus approach. *Physica A: Statistical Mechanics and its Applications*, 564:125502, 2021.
- [42] Lauren A. Rivera. Hiring as cultural matching: The case of elite professional service firms. *American Sociological Review*, 77(6):999–1022, 2012.
- [43] Roberto M. Rubineau, Brian Fernandez. Tipping Points: Referral Homophily and Job Segregation — dspace.mit.edu. <https://dspace.mit.edu/handle/1721.1/66931>. [Accessed 20-01-2024].
- [44] Jad Salem, Deven Desai, and Swati Gupta. Don't let Ricci v. DeStefano hold you back: A bias-aware legal solution to the hiring paradox. In *Facct*, pages 651–666, 2022.
- [45] Roberta Sinatra, Dashun Wang, Pierre Deville, Chaoming Song, and Albert-László Barabási. Quantifying the evolution of individual scientific impact. *Science*, 354(6312):aaf5239, 2016.

- [46] Ana-Andreea Stoica, Jessy Xinyi Han, and Augustin Chaintreau. Seeding network influence in biased networks and the benefits of diversity. In *WWW*, pages 2089–2098. ACM / IW3C2, 2020.
- [47] Tom Sühr, Sophie Hilgard, and Himabindu Lakkaraju. Does fair ranking improve minority outcomes? understanding the interplay of human and algorithmic biases in online hiring. In *AIES*, pages 989–999, 2021.
- [48] Phyllis Tharenou. Explanations of managerial career advancement. *Australian Psychologist*, 32(1):19–28, 1997.
- [49] Zijian Wang and David Jurgens. It's going to be okay: Measuring access to support in online communities. In Ellen Riloff, David Chiang, Julia Hockenmaier, and Jun'ichi Tsujii, editors, *Proceedings of the 2018 Conference on Empirical Methods in Natural Language Processing*, Brussels, Belgium, 2018. Association for Computational Linguistics.

A Appendix

A.1 Proof of Lemma 5.2:

Before we prove the bounds on the ϕ_t process itself, we first must prove bounds on $\mathbb{E} \left[\frac{R_t}{R_t + B_t} \right]$, as defined in the following Lemma.

Lemma A.1. Assume $\exists \varepsilon \in (0, \frac{1}{2})$ such that $\left(\frac{1}{n_t} \right)^{\frac{1}{2} - \varepsilon} \leq \phi_t \leq \frac{1}{2}$. Then there exists N_0 such that for $n_t \geq N_0$ the following holds

$$\left(1 - \frac{1}{n_{t-1}^{\varepsilon/4}} \right) \frac{\mathbb{E}[R_t]}{\mathbb{E}[R_t + B_t]} < \frac{R_t}{R_t + B_t} < \left(1 + \frac{1}{n_{t-1}^{\varepsilon/4}} \right) \frac{\mathbb{E}[R_t]}{\mathbb{E}[R_t + B_t]}. \quad (45)$$

With probability at least $1 - \frac{8}{\exp(C_1 n_{t-1}^\varepsilon)}$, where $C_1 = \min \left\{ \frac{\mu_{RR}}{24}, \frac{\mu_{RB}}{12} \right\}$ and $\varepsilon \in (0, \frac{1}{2})$. Additionally, we have

$$\left(1 - \frac{1}{n_{t-1}^{\varepsilon/5}} \right) \frac{\mathbb{E}[R_t]}{\mathbb{E}[R_t + B_t]} \leq \mathbb{E} \left[\frac{R_t}{R_t + B_t} \right] \leq \left(1 + \frac{1}{n_{t-1}^{\varepsilon/5}} \right) \frac{\mathbb{E}[R_t]}{\mathbb{E}[R_t + B_t]}. \quad (46)$$

Prerequisite (Chernoff Bound). We define a Chernoff Bound [29] on a random variable X :

$$\Pr(X \geq \delta) \leq \mathbb{E}[e^{sX}]e^{-s\delta}. \quad (47)$$

For all $s > 0$. A corollary of this is also

$$\Pr(|X - \mathbb{E}[X]| \geq \delta \mathbb{E}[X]) \leq 2e^{-\delta^2 \mathbb{E}[X]/3}. \quad (48)$$

□

Proof of Lemma A.1. Consider random variables RR, RB, BB , representing the total weight of Red-Red, Red-Blue, and Blue-Blue edges respectively. We can bound the number of these edges (RR/w_{RR}), (RB/w_{RB}) using the Chernoff Bound

$$\begin{cases} \Pr \left(\left| \frac{RR}{w_{RR}} - \frac{\mathbb{E}[RR]}{w_{RR}} \right| \geq \delta \frac{\mathbb{E}[RR]}{w_{RR}} \right) \leq 2 \exp \left(-\frac{\delta^2}{6} (n_t^R)^2 \Pi_{RR}(t) \right) \\ \Pr \left(\left| \frac{RB}{w_{RB}} - \frac{\mathbb{E}[RB]}{w_{RB}} \right| \geq \delta \frac{\mathbb{E}[RB]}{w_{RB}} \right) \leq 2 \exp \left(-\frac{\delta^2}{6} (n_t^R n_t^B) \Pi_{RB}(t) \right) \end{cases}. \quad (49)$$

From our assumption, we find that $n_t^R \geq n_t^{\frac{1}{2} + \varepsilon}$ where $\varepsilon \in (0, \frac{1}{2})$, and $n_t^B \geq \frac{n_t}{2}$. Define constant $C_1 = \min \left\{ \frac{\mu_{RR}}{24}, \frac{\mu_{RB}}{12} \right\}$. Letting $\delta = \frac{1}{n_t^{\varepsilon/2}}$, we can establish the following probability bounds on edge weights RR, RB, BB :

$$\Pr \left(|RR - \mathbb{E}[RR]| \geq \frac{\mathbb{E}[RR]}{n_t^{\varepsilon/2}} \right) \leq 2 \exp \left(-\frac{n_t \Pi_{RR}(t)}{6} n_t^\varepsilon \right) \leq 2 \exp(-C_1 n_t^\varepsilon). \quad (50)$$

$$\Pr \left(|RB - \mathbb{E}[RB]| \geq \frac{\mathbb{E}[RB]}{n_t^{\varepsilon/2}} \right) \leq 2 \exp \left(-\frac{n_t \Pi_{RB}(t)}{12} n_t^{\frac{1}{2}} \right) \leq 2 \exp(-C_1 n_t^\varepsilon). \quad (51)$$

$$Pr \left(|BB - \mathbb{E}[BB]| \geq \frac{\mathbb{E}[BB]}{n_t^{\varepsilon/2}} \right) \leq 2 \exp \left(-\frac{n_t \Pi_{BB}(t)}{24} n_t^{1-\varepsilon} \right) \leq 2 \exp(-C_1 n_t^\varepsilon). \quad (52)$$

See that $R_t = RR_t + RB_t$, so we can establish bounds on the total weight of red R by union bound

$$Pr \left(|R - \mathbb{E}[R]| \geq \frac{\mathbb{E}[R]}{n_t^{\varepsilon/2}} \right) \leq 4 \exp(-C_1 n_t^\varepsilon). \quad (53)$$

Likewise for the total blue weight B

$$Pr \left(|B - \mathbb{E}[B]| \geq \frac{\mathbb{E}[B]}{n_t^{\varepsilon/2}} \right) \leq 4 \exp(-C_1 n_t^\varepsilon). \quad (54)$$

We see that the event $|R - \mathbb{E}[R]| < \frac{\mathbb{E}[R]}{n_t^{\varepsilon/2}}$ implies $\left(1 - \frac{1}{n_t^{\varepsilon/2}}\right) \mathbb{E}[R] < R < \left(1 + \frac{1}{n_t^{\varepsilon/2}}\right) \mathbb{E}[R]$, so we use this to bound our ratio $\frac{R}{R+B}$

$$\left(\frac{\left(1 - \frac{1}{n_t^{\varepsilon/2}}\right)}{\left(1 + \frac{1}{n_t^{\varepsilon/2}}\right)} \right) \frac{\mathbb{E}[R]}{\mathbb{E}[R+B]} < \frac{R}{R+B} < \left(\frac{\left(1 + \frac{1}{n_t^{\varepsilon/2}}\right)}{\left(1 - \frac{1}{n_t^{\varepsilon/2}}\right)} \right) \frac{\mathbb{E}[R]}{\mathbb{E}[R+B]} \quad (55)$$

$$\left(1 - \frac{1}{n_t^{\varepsilon/4}}\right) \frac{\mathbb{E}[R]}{\mathbb{E}[R+B]} < \frac{R}{R+B} < \left(1 + \frac{1}{n_t^{\varepsilon/4}}\right) \frac{\mathbb{E}[R]}{\mathbb{E}[R+B]}. \quad (56)$$

Define event \mathcal{G} as the event of this inequality holding. By union bound on the values from (53) and (54), we see that $Pr(\mathcal{G}^C) \leq 8 \exp(-C_1 n_t^\varepsilon)$. Therefore our inequality holds with probability at least $1 - \frac{8}{\exp(C_1 n_t^\varepsilon)}$, concluding the proof for inequality (45).

To prove the second inequality (46), we extend our bound to the expected value $\mathbb{E} \left[\frac{R_t}{R_t+B_t} \right]$. Notice our ratio $0 < \frac{R_t}{R_t+B_t} < 1$, so to upper bound our expectation we condition on our inequality \mathcal{G} from (56).

$$\mathbb{E} \left[\frac{R_t}{R_t+B_t} \right] \leq \left(\left(1 + \frac{1}{n_t^{\varepsilon/4}}\right) \frac{\mathbb{E}[R]}{\mathbb{E}[R+B]} \right) Pr(\mathcal{G}) + 1 \cdot (1 - Pr(\mathcal{G})) \quad (57)$$

$$\leq \left(1 - \frac{8}{\exp(C_1 n_t^\varepsilon)}\right) \left(1 + \frac{1}{n_t^{\varepsilon/4}}\right) \frac{\mathbb{E}[R]}{\mathbb{E}[R+B]} + \frac{8}{\exp(C_1 n_t^\varepsilon)} \quad (58)$$

$$\leq \left(1 + \frac{1}{n_t^{\varepsilon/4}}\right) \frac{\mathbb{E}[R]}{\mathbb{E}[R+B]} + \frac{8}{\exp(C_1 n_t^\varepsilon)} \quad (59)$$

$$\leq \left(1 + \frac{1}{n_t^{\varepsilon/5}}\right) \frac{\mathbb{E}[R]}{\mathbb{E}[R+B]}. \quad (60)$$

This above inequality only holds when $n_t \geq N_0$. Therefore, defining constants N_1, N_2

$$N_1: \text{ When } n_t \geq N_1 = \exp \left(\frac{20 \ln 2}{\varepsilon} \right) \text{ then } \frac{1}{n_t^{\varepsilon/5}} - \frac{1}{n_t^{\varepsilon/4}} \geq \frac{1}{n_t^{\varepsilon/4}}$$

$$N_2: n_t^\varepsilon \geq \ln(n_t) \left(\frac{2-3\varepsilon}{4C_1} \right) + \frac{\ln 2}{4C_1} - \frac{1}{C} \ln \left(\frac{\mu_{RB} w_{RB}}{5\mu_{RR} w_{RR} + 4\mu_{RB} w_{RB}} \right)$$

Thus, let $N_0 = \max\{N_1, N_2\}$ so that for $n_t \geq N_0$ both bounds hold, completing the proof for the upper bound. Now to prove the lower bound, we condition again

$$\mathbb{E} \left[\frac{R_t}{R_t + B_t} \right] \geq \left(\left(1 - \frac{1}{n_t^{\varepsilon/4}} \right) \frac{\mathbb{E}[R]}{\mathbb{E}[R + B]} \right) Pr(\mathcal{G}) + 0 \cdot (1 - Pr(\mathcal{G})) \quad (61)$$

$$\geq \left(1 - \frac{8}{\exp(C_1 n_t^\varepsilon)} \right) \left(1 - \frac{1}{n_t^{\varepsilon/4}} \right) \frac{\mathbb{E}[R]}{\mathbb{E}[R + B]} \quad (62)$$

$$\geq_{N_3} \left(1 - \frac{1}{n_t^{\varepsilon/5}} \right) \frac{\mathbb{E}[R]}{\mathbb{E}[R + B]}. \quad (63)$$

There exists N_3 such that inequality (63) holds for $n_t \geq N_3$

$$\left(1 - \frac{8}{\exp(8C_1 n_t^\varepsilon)} \right) \left(1 - \frac{1}{n_t^{\varepsilon/4}} \right) \geq 1 - \frac{1}{n_t^{\varepsilon/5}}. \quad (64)$$

Thus let $N_0 \geq \max\{N_1, N_2, N_3\}$ such that all our bounds hold for $n_t \geq N_0$ and we have

$$\left(1 - \frac{1}{n_t^{\varepsilon/5}} \right) \frac{\mathbb{E}[R_t]}{\mathbb{E}[R_t + B_t]} \leq \mathbb{E} \left[\frac{R_t}{R_t + B_t} \right] \leq \left(1 + \frac{1}{n_t^{\varepsilon/5}} \right) \frac{\mathbb{E}[R_t]}{\mathbb{E}[R_t + B_t]}. \quad (65)$$

Concluding the proof of (46). \square

Now with Lemma A.1 we can prove Lemma 5.2.

Proof of Lemma 5.2 Consider the expected number of new red nodes arriving at time $t + 1$, denoted $\mathbb{E}[m_{t+1}^R]$, we can bound this quantity by rounding our total expected new nodes λn_t

$$\lfloor \lambda n_t \rfloor \mathbb{E} \left[\frac{R_t}{R_t + B_t} \right] \leq \mathbb{E}[m_{t+1}^R | \mathcal{F}_t] \leq \lceil \lambda n_t \rceil \mathbb{E} \left[\frac{R_t}{R_t + B_t} \right]. \quad (66)$$

Additionally, we can use inequality (46) from Theorem 1 to bound $\mathbb{E} \left[\frac{R_t}{R_t + B_t} \right]$

$$\lfloor \lambda n_t \rfloor \left(1 - \frac{1}{n_t^{\varepsilon/5}} \right) \frac{\mathbb{E}[R_t]}{\mathbb{E}[R_t + B_t]} \leq \mathbb{E}[m_{t+1}^R | \mathcal{F}_t] \leq \lceil \lambda n_t \rceil \left(1 + \frac{1}{n_t^{\varepsilon/5}} \right) \frac{\mathbb{E}[R_t]}{\mathbb{E}[R_t + B_t]}. \quad (67)$$

Also note that we define $\Gamma_q(\phi_t) := \frac{\mathbb{E}[R_t]}{\mathbb{E}[R_t + B_t]}$

$$\frac{\mathbb{E}[R_t]}{\mathbb{E}[R_t + B_t]} = \frac{(n_t^R)^2 w_{RR} \Pi_{RR}(t) + (n_t^R n_t^B) w_{RB} \Pi_{RB}(t)}{((n_t^R)^2 + (n_t^B)^2) w_{RR} \Pi_{RR}(t) + 2(n_t^R n_t^B) w_{RB} \Pi_{RB}(t)} \quad (68)$$

$$= \frac{\phi_t w_{RR} \Pi_{RR}(t) + \phi_t (1 - \phi_t) w_{RB} \Pi_{RB}(t)}{(\phi_t^2 + (1 - \phi_t)^2) w_{RR} \Pi_{RR}(t) + 2\phi_t (1 - \phi_t) w_{RB} \Pi_{RB}(t)} \quad (69)$$

$$= \Gamma_q(\phi_t). \quad (70)$$

Using this to bound our original equation for $\mathbb{E}[\phi_{t+1} | \mathcal{F}_t] = \frac{n_t^R + \mathbb{E}[m_{t+1}^R | \mathcal{F}_t]}{(1 + \lambda)n_t}$

$$\frac{\phi_t + \frac{\lfloor \lambda n_t \rfloor}{n_t} \left(1 - \frac{1}{n_t^{\varepsilon/5}} \right) \cdot \Gamma_q(\phi_t)}{1 + \frac{\lfloor \lambda n_t \rfloor}{n_t}} \leq \mathbb{E}[\phi_{t+1} | \mathcal{F}_t] \leq \frac{\phi_t + \frac{\lceil \lambda n_t \rceil}{n_t} \left(1 + \frac{1}{n_t^{\varepsilon/5}} \right) \cdot \Gamma_q(\phi_t)}{1 + \frac{\lceil \lambda n_t \rceil}{n_t}}. \quad (71)$$

As $t \rightarrow \infty$, our bounds converge to the following expression

$$\mathbb{E}[\phi_{t+1} | \mathcal{F}_t] = \frac{\phi_t + \lambda \cdot \Gamma_q(\phi_t)}{1 + \lambda}. \quad (72)$$

Which is our deterministic approximation, concluding the proof. \square

A.2 Derivation of Deterministic Approximation

Using Theorem 5.1 we define $\Pi_{RR}(t), \Pi_{RB}(t), \Pi_{BB}(t)$, where for Red-Blue edges:

$$\Pi_{RB}(t) = \frac{\mu_{RB}}{n_t} + \sum_{k=0}^{t-1} \frac{\mu_{RB}}{n_k} \prod_{j=k+1}^t q \left(1 - \frac{\mu_{RB}}{n_j} \right). \quad (73)$$

And for Blue-Blue edges:

$$\Pi_{BB}(t) = \frac{\mu_{BB}}{n_t} + \sum_{k=0}^{t-1} \frac{\mu_{BB}}{n_k} \prod_{j=k+1}^t q \left(1 - \frac{\mu_{BB}}{n_j} \right). \quad (74)$$

In our graph, the existence of an edge is not dependent on the existence of any other edges, so our probability is independent across edges. As such, we define the expected weight of Red and Blue nodes at time t as the expected weight of all Red-Red, Red-Blue, and Blue-Blue edges in our graph.

$$\mathbb{E}[R_t] = n_t^R \Pi_{RR}(t) w_{RR} + \frac{(n_t^R)(n_t^R - 1)}{2} 2w_{RR} \Pi_{RR}(t) + n_t^R n_t^B w_{RB} \Pi_{RB}(t) \quad (75)$$

$$= (n_t^R)^2 \Pi_{RR}(t) w_{RR} + (n_t^R + n_t^B) \Pi_{RB}(t) w_{RB} \quad (76)$$

$$\mathbb{E}[B_t] = n_t^B \Pi_{BB}(t) w_{BB} + \frac{(n_t^B)(n_t^B - 1)}{2} 2w_{BB} \Pi_{BB}(t) + n_t^R n_t^B w_{RB} \Pi_{RB}(t) \quad (77)$$

$$= (n_t^B)^2 w_{BB} \Pi_{BB}(t) + n_t^R n_t^B w_{RB} \Pi_{RB}(t). \quad (78)$$

Assume $\mathbf{P} = \begin{bmatrix} \mu_{RR} & \mu_{RB} \\ \mu_{RB} & \mu_{RR} \end{bmatrix}$, $\mathbf{W} = \begin{bmatrix} w_{RR} & w_{RB} \\ w_{RB} & w_{RR} \end{bmatrix}$. With this, we calculate $\frac{\mathbb{E}[R_t]}{\mathbb{E}[R_t + B_t]}$

$$\frac{\mathbb{E}[R_t]}{\mathbb{E}[R_t + B_t]} = \frac{(n_t^R)^2 w_{RR} \Pi_{RR}(t) + (n_t^R n_t^B) w_{RB} \Pi_{RB}(t)}{((n_t^R)^2 + (n_t^B)^2) w_{RR} \Pi_{RR}(t) + 2(n_t^R n_t^B) w_{RB} \Pi_{RB}(t)}. \quad (79)$$

Let ϕ_t be the fraction of red nodes and m_t be the new nodes joining the graph at time t . From our growth dynamics we know $\phi_t = \frac{n_{t-1}^R + m_t^R}{n_{t-1} + m_t}$. Note that while n_t^R and m_t^R are random variables, n_t and m_t are deterministic. We can approximate this expectation

$$\mathbb{E}[\phi_{t+1} | \mathcal{F}_t] = \frac{n_t^R + \lambda n_t \mathbb{E} \left[\frac{R_t}{R_t + B_t} \right]}{(1 + \lambda) n_t} \approx \frac{n_t^R + \lambda n_t \frac{\mathbb{E}[R_t]}{\mathbb{E}[R_t + B_t]}}{(1 + \lambda) n_t} \approx \frac{\phi_t + \lambda \cdot \Gamma_q(\phi_t)}{1 + \lambda}. \quad (80)$$

Where

$$\Gamma_q(x_t) = \frac{x_t^2 w_{RR} \Pi_{RR}(t) + x_t(1 - x_t) w_{RB} \Pi_{RB}(t)}{(x_t^2 + (1 - x_t)^2) w_{RR} \Pi_{RR}(t) + 2x_t(1 - x_t) w_{RB} \Pi_{RB}(t)}. \quad (81)$$

A.3 Proof of Lemma 6.4:

Proof. For convenience, define $r := 1 + \lambda$. Note that $n_t = n_0 r^t$. Considering the definitions of $\Pi_{RR}(t), \Pi_{RB}(t)$ from Lemma 5.1 we can expand ρ_t as follows

$$\rho_t = \frac{w_{RR}\Pi_{RR}(t)}{w_{RB}\Pi_{RB}(t)} \quad (82)$$

$$= \frac{w_{RR} \left(\mu_{RR} + \mu_{RR} r^t \sum_{k=0}^{t-1} r^{-k} \prod_{j=k+1}^t q \left(1 - \frac{\mu_{RR}}{n_0} r^{-j} \right) \right)}{w_{RB} \left(\mu_{RB} + \mu_{RB} r^t \sum_{k=0}^{t-1} r^{-k} \prod_{j=k+1}^t q \left(1 - \frac{\mu_{RB}}{n_0} r^{-j} \right) \right)} \quad (83)$$

$$= \frac{w_{RR} \left(\mu_{RR} r^t \sum_{k=0}^t r^{-k} \prod_{j=k+1}^t q \left(1 - \frac{\mu_{RR}}{n_0} r^{-j} \right) \right)}{w_{RB} \left(\mu_{RB} r^t \sum_{k=0}^t r^{-k} \prod_{j=k+1}^t q \left(1 - \frac{\mu_{RB}}{n_0} r^{-j} \right) \right)} \quad (84)$$

$$= \frac{w_{RR}\mu_{RR} \left(\sum_{k=0}^t r^{-k} \prod_{j=k+1}^t q \left(1 - \frac{\mu_{RR}}{n_0} r^{-j} \right) \right)}{w_{RB}\mu_{RB} \left(\sum_{k=0}^t r^{-k} \prod_{j=k+1}^t q \left(1 - \frac{\mu_{RB}}{n_0} r^{-j} \right) \right)} \quad (85)$$

$$= \frac{w_{RR}\mu_{RR} \left(\sum_{k=0}^t r^{-k} q^{t-k-1} \prod_{j=k+1}^t \left(1 - \frac{\mu_{RR}}{n_0} r^{-j} \right) \right)}{w_{RB}\mu_{RB} \left(\sum_{k=0}^t r^{-k} q^{t-k-1} \prod_{j=k+1}^t \left(1 - \frac{\mu_{RB}}{n_0} r^{-j} \right) \right)} \quad (86)$$

$$= \frac{w_{RR}\mu_{RR} q^{t-1} \left(\sum_{k=0}^t (rq)^{-k} \prod_{j=k+1}^t \left(1 - \frac{\mu_{RR}}{n_0} r^{-j} \right) \right)}{w_{RB}\mu_{RB} q^{t-1} \left(\sum_{k=0}^t (rq)^{-k} \prod_{j=k+1}^t \left(1 - \frac{\mu_{RB}}{n_0} r^{-j} \right) \right)} \quad (87)$$

$$= \frac{w_{RR}\mu_{RR} \left(\sum_{k=0}^t (rq)^{-k} \prod_{j=k+1}^t \left(1 - \frac{\mu_{RR}}{n_0} r^{-j} \right) \right)}{w_{RB}\mu_{RB} \left(\sum_{k=0}^t (rq)^{-k} \prod_{j=k+1}^t \left(1 - \frac{\mu_{RB}}{n_0} r^{-j} \right) \right)}. \quad (88)$$

Define $S_{RR}(t) := \sum_{k=0}^t (rq)^{-k} \prod_{j=k+1}^t \left(1 - \frac{\mu_{RR}}{n_0} r^{-j} \right)$, and define $S_{RB}(t)$ similarly. Since we assume $rq > 1$, we see that $S_{RR}(t)$ is a partial geometric series, or that $S_{RR}(t) \leq \sum_{k=0}^t (rq)^{-k} \leq \frac{1+\lambda}{\lambda}$. Therefore, $S_{RR} := \lim_{t \rightarrow \infty} S_{RR}(t)$ exists and can be defined as

$$S_{RR} = \sum_{k=0}^{\infty} (q(1+\lambda))^{-k} \prod_{j=k+1}^{\infty} \left(1 - \frac{\mu_{RR}}{n_0} (1+\lambda)^{-j} \right), \quad (89)$$

$$S_{RB} = \sum_{k=0}^{\infty} (q(1+\lambda))^{-k} \prod_{j=k+1}^{\infty} \left(1 - \frac{\mu_{RB}}{n_0} (1+\lambda)^{-j} \right), \quad (90)$$

concluding the proof. To our knowledge, there are no explicit solutions for S_{RR}, S_{RB} . \square